

Contents

<i>Section</i>	<i>Page</i>
Summary	1 1/A7
Introduction	1 1/A7
Radiance	2 1/A8
Noise Equivalent Radiance	2 1/A8
Reflectance	3 1/A9
Noise Equivalent Reflectance	4 1/A10
Relationship of NER to NE $\Delta\rho$	4 1/A10
Determination of NE $\Delta\rho$	5 1/A11
Atmospheric Influence	8 1/A14
Direct Measurement of NE $\Delta\rho$	15 1/B7
Comparison of Measured and Calculated NE $\Delta\rho$	18 1/B10
Conclusion	19 1/B11
Appendix A—Meteorological Effects on Radiation	21 1/B13
Appendix B—Symbols	23 1/C1
References	26 1/C4

JAN 7 1980

Item 830-H-15

NAS 1.60: 1575

COMPLETED

NASA Technical Paper 1575

Determination of Noise Equivalent
Reflectance for a Multispectral
Scanner - A Scanner Sensitivity Study

ORIGINAL

Daniel E. Gibbons and Richard R. Richard

DECEMBER 1979

NASA

(32)

NASA Technical Paper 1575

Determination of Noise Equivalent
Reflectance for a Multispectral
Scanner - A Scanner Sensitivity Study

Daniel E. Gibbons

Fort Lewis College

Durango, Colorado

Richard R. Richard

Lyndon B. Johnson Space Center

Houston, Texas

NASA

National Aeronautics
and Space Administration

Scientific and Technical
Information Branch

15 79

Contents

<i>Section</i>	<i>Page</i>
Summary	1
Introduction	1
Radiance	2
Noise Equivalent Radiance	2
Reflectance	3
Noise Equivalent Reflectance	4
Relationship of NER to NE $\Delta\rho$	4
Determination of NE $\Delta\rho$	5
Atmospheric Influence	8
Direct Measurement of NE $\Delta\rho$	15
Comparison of Measured and Calculated NE $\Delta\rho$	18
Conclusion	19
Appendix A—Meteorological Effects on Radiation	21
Appendix B—Symbols	23
References	26

Tables

<i>Table</i>	<i>Page</i>
I Solar Irradiance at Sea Level on an Area Normal to the Sun	7
II Noise Equivalent Radiance	8
III M ² S Bandwidths	8
IV Tabulation of NE $\Delta\rho$	8
V Solar Spectral Irradiance—Proposed Standard Curve	9
VI Standard Values of the Turbidity Coefficient <i>B</i> as a Function of Latitude and Altitude	11
VII Summary of Available Meteorological Data for Flight Dates	13
VIII Possible Variations in Calculated Values of NE $\Delta\rho$ for Channel 4 of the M ² S	19

Figures

<i>Figure</i>		<i>Page</i>
1	Schematic diagram showing coordinate system and major parameters	3
2	Diagram of system linear in reflectance	4
3	Ratio of diffuse irradiance to solar irradiance as a function of wavelength	12
4	Variation of visual range with extinction coefficient at a wavelength of 0.55 micrometer ..	13
5	Dependence of total Rayleigh optical depth τ_R on wavelength	14
6	Aerosol optical depth τ_a as a function of visual range R_v . Parameter is spectral wavelength λ in micrometers	14
7	Air mass m as a function of time	15
8	Nomograph of scanner parameters for haze condition; visibility = 4 kilometers	15
9	Nomograph of scanner parameters for clear condition; visibility = 15 kilometers	16
10	Nomograph of scanner parameters for exceptionally clear condition; visibility = 100 kilometers	16
11	Reflectance as a function of wavelength for 5-, 8-, 16-, and 28-percent-reflectance panels (September 25, 1975)	16
12	Reflectance as a function of center wavelength for 60-percent-reflectance panel (September 25, 1975)	16
13	Sample printout of M ² S data showing clustering method used for locating reflectance panel data	17
14	Plot of scene signal voltage as a function of relative reflectance for channel 7 (September 25, 1975)	17
15	Plot of relative reflectance as a function of scene signal voltage for channel 3 (September 25, 1975)	18
16	Scanner video trace	18
17	Geometric relationships of solar irradiance quantities used in Schwarzschild's equation	21

Determination of Noise Equivalent Reflectance for a Multispectral Scanner—A Scanner Sensitivity Study

By Daniel E. Gibbons* and Richard R. Richard

Summary

Airborne remote sensor scanner data were acquired over calibrated targets on four different occasions, providing a measurement of scanner sensitivity under operational conditions. These measurements were then compared with predicted sensitivity values based on more or less standard calculations, one of which is performed assuming two sets of atmospheric conditions and a 45° Sun angle and two of which are based on atmospheric models attributable to Turner and to Ångström. The comparisons show that, on the average, although the potential for best accuracy lies in the atmospherically corrected values, the assumed conditions produce good results adequate for many purposes.

A nomograph was developed to provide a means of predicting the variations in noise equivalent reflectance that are due to time of day, seasons, and latitude. Because of the extremes in values which are evident, the nomograph should prove useful to investigators whose requirements are stringent and who are faced with the use of marginally sensitive remote-sensing equipment.

Introduction

Users of airborne remote sensor scanner data are frequently concerned with the characterization of ground targets through the measurement of variations in target reflectance. Because the variations of interest are often small in magnitude and are difficult to measure precisely, considerable interest is created in the definition and measurement of the capability of a sensor to respond to small reflectance changes. This capability, related to sensi-

tivity, is often described in terms of noise equivalent reflectance $NE \Delta\rho$, which is the minimum detectable variation in reflectance and is thus defined as the resolution of the system.

Several methods can be used to measure or calculate this sensitivity parameter, each fraught with its own set of problems. Because of problems, mostly logistical, the usual approach is to perform a calculation on the basis of certain assumed target conditions. It is these assumed target conditions, which are not universally agreed upon, that are responsible for the variety of sensitivity numbers assigned to a particular instrument by various working groups. The possibility of improving this situation was one of the prime movers in this study, which was conducted during the summers of 1977 and 1978. The objectives were to perform measurements of $NE \Delta\rho$ and to compare these values with mathematically predictable values, to ascertain the range of values possible under normal operating conditions, and then to determine what conditions should be assumed or what approach should be taken to calculate the most realistic or meaningful values of $NE \Delta\rho$.

As previously stated, data users prefer noise equivalent reflectance as a sensitivity parameter. Sensor engineers, on the other hand, prefer a different sensitivity parameter, noise equivalent radiance (NER). This preference for NER is motivated by the straightforwardness of the measurement process, which is accomplished with a minimum of equipment of a variety found in most optical laboratories.

The first part of this report contains a limited review of terminology as an aid to those who may not be thoroughly familiar with, or may have forgotten, some of the material. Additional information on atmospheric modeling is provided in appendix A.

In compliance with the NASA's publication policy, the original units of measure have been converted to the equivalent value in the Système Inter-

*Fort Lewis College, Durango, Colorado.

national d'Unités (SI). As an aid to the reader, the SI units are written first and the original units are written parenthetically thereafter.

Radiance

The detectors used in remote sensor systems respond to the time rate of transfer of radiant energy (also called radiant flux, expressed in watts). The most easily visualized flux measurement situation is one in which the energy-collecting aperture of a detector is completely filled by radiation of uniform density. Such a situation is realized in the use of a term called irradiance H , which is radiant flux per unit area incident on a surface given in watts per square centimeter. The input radiant power P_{in} (watts) is simply the product of irradiance and collecting area A_c .

$$P_{in} = H \cdot A_c \quad (1)$$

A calibrated system, then, enables the measurement of H and thereby makes the remote-sensing problem one of properly relating target characteristics to H , with due consideration of the transmitting or intervening medium.

Target characteristics are approached through the concept of radiance N , which is the amount of power from a source of unit area radiated into a unit solid angle in watts per square centimeter per steradian. Radiance N and irradiance H are related in the following way.

$$H = N\omega \quad (2)$$

where ω is the viewing angle of the detector system in steradians. Thus, it can be seen, ignoring atmospheric attenuation for the time being, that the power density H measured by the detector system is related to a target characteristic N through a detector system characteristic ω . The parameters H and N are also defined as follows (e.g., ref. 1).

$$H = \frac{\partial P}{\partial A_c}; \quad N = \frac{\partial^2 P}{\partial \omega \partial A_t}$$

where the quantities are defined in appendix B.

Noise Equivalent Radiance

The NER of a scanner system is defined as the amount of change in radiance required to produce a signal equivalent to the noise of the system. Stated another way, this is the quantity of radiance that produces a signal-to-noise ratio (S/N) of unity. The radiance for a signal of this level is difficult to measure, and, for a linear system, a larger radiance change is used to determine NER.

$$NER = \frac{\Delta N_s}{\left(\frac{V_s}{V_n}\right)} \quad (3)$$

where ΔN_s is the change in scene radiance, V_s is the signal voltage proportional to the scene radiance change, and V_n is the noise voltage. An input radiance change that will produce an output signal equal to the noise (S/N = 1) is the minimum detectable change in radiance level. Thus, NER is the minimum detectable radiance and is defined as the resolution of the system.

The airborne scanners currently in use at the NASA Lyndon B. Johnson Space Center (JSC) use mechanical means to generate ground scene video data; that is, a rotating mirror is used to reflect a small element of the target scene viewed by a narrow-angle telescope. The image from the telescope is then spectrally dispersed onto detectors that produce voltages proportional to the collected spectral radiant power. The mirror rotation is continuous so that the interior of the scanner, which contains visible and infrared calibration sources, is viewed by the detectors once for each revolution of the rotating scan mirror. The internal visible calibration source provides one means of obtaining the radiance change required by equation (3). In this application, one of the internal blackbodies is used to provide a zero-radiance (in the visible spectrum) target. Since the radiance value of the calibration source is known, calculation of NER for a linear system is a simple matter of measuring the change in the output signal caused by viewing first the blackbody and then the calibration source and, then, of measuring the noise signal. The NER calculation is completed by ratioing the signal and noise output voltages and dividing into the value

for radiance of the internal calibration source (from eq. (3)).

$$\begin{aligned} \text{NER} &= \frac{\Delta N_s}{\left(\frac{V_s}{V_n}\right)} \\ &= \frac{N_2 - N_1}{S/N} \\ &= \frac{N_2 - 0}{S/N} \end{aligned}$$

A preferred way to measure NER is to use a more accurate laboratory source as the target. The reason for this preference is that, in some scanners, the internal calibration source optics train is not the same as the target-viewing optics train, and viewing the known radiance source through an optics train identical to that through which the ground target is viewed eliminates this possible source of error.

Reflectance

Reflectance is defined as the ratio of the radiant flux reflected by a body to that incident upon it. Thus, the computation or measurement of reflectance, at least in principle, is a straightforward process. In practice, however, the measurement problem is complicated by such considerations as surface irregularities which scatter the incident energy in many, perhaps all, directions with perhaps some spatial preference.

Other possible complications are the wavelength dependence of the measuring devices and the impracticality of always knowing the magnitude of the incident radiation. These complications are addressed and minimized as necessary, according to the requirements of the experimenter. However, generalizations or simplifying assumptions can be made regarding the character of targets and measurement geometry, particularly as related to reflectance and wavelength dependence. One derivation (ref. 2), leading to an estimation of power received by the detector, relates the incident power on a differential area dA to that reflected from the area

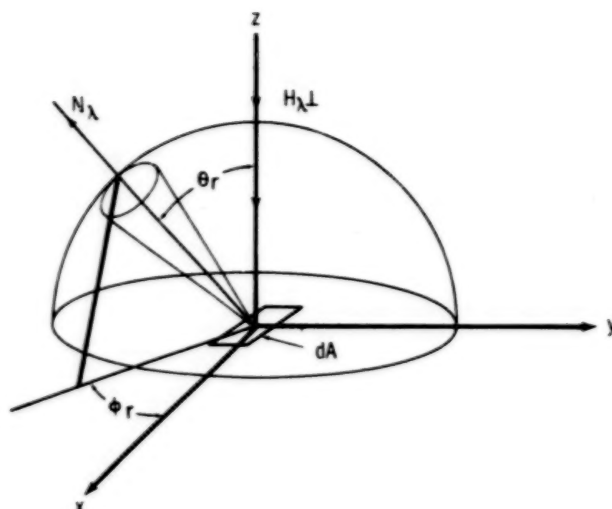


FIGURE 1.—Schematic diagram showing coordinate system and major parameters.

in a given direction and thereby gives rise to the idea of directional dependence. In general, the amount of radiation collected will depend on the direction in which the detector views the target (fig. 1). Thus, a partial reflectance ρ' is defined as the ratio of the spectral radiance N_λ reflected in a given direction from a surface to the spectral normal irradiance $H_{\lambda\perp}$ on an area dA . This ratio can be expressed as

$$\rho'(\theta_r, \phi_r) = \frac{N_\lambda}{H_{\lambda\perp}} \quad (4)$$

where $H_{\lambda\perp} = (dP_i/dA)$ equals the irradiance perpendicular to the target and is incident power on dA .

A perfectly diffusing surface is one from which equal amounts of energy are reflected in all directions by an incident beam. Such a surface would appear equally bright to a detector when viewed from any direction. Perfectly diffusing surfaces are assumed in this report, and they result in a simple relation between total reflectance and partial reflectance.

The power reflected from the surface dP_r (fig. 1) can be expressed as

$$dP_r = dA \int_h N_\lambda d\Omega \quad (5)$$

where $d\Omega$ is the projected solid angle defined as

$$d\Omega = \cos \theta \sin \theta d\theta d\phi \quad (6)$$

and \int_h indicates an integration over the entire hemisphere above the area dA . Substituting equations (4) and (6) into equation (5),

$$dP_r = dA \int_0^{\pi/2} \int_0^{2\pi} \rho' H_{\lambda \perp} \cos \theta \sin \theta d\theta d\phi \quad (7)$$

$$dP_r = dA \int_0^{\pi/2} \int_0^{2\pi} \rho' \left(\frac{dP_i}{dA} \right) \cos \theta \sin \theta d\theta d\phi \quad (8)$$

Because the surface is diffuse, ρ' is equal to a constant. Hence, equation (8) becomes

$$dP_r = \pi \rho' dP_i \quad (9)$$

Finally, the ratio of dP_r/dP_i is defined as the total reflectance ρ , related to the partial reflectance factor for diffuse surfaces (eq. (9)) as given by

$$\rho = \pi \rho' \quad (10)$$

Substituting equation (10) into equation (4),

$$N_{\lambda} = \frac{\rho}{\pi} H_{\lambda \perp} \quad (11)$$

If the irradiance on the surface dA is at some angle θ_0 measured with respect to the zenith, or a point directly overhead, then,

$$H_{\lambda \perp} = H_{\lambda} \cos \theta_0 \quad (12)$$

Finally, substituting equation (12) into equation (11),

$$N_{\lambda} = \frac{\rho}{\pi} H_{\lambda} \cos \theta_0 \quad (13)$$

If a perfectly diffusing target surface is assumed, equation (13) provides a useful relationship among target radiance, total reflectance, and irradiance.

Noise Equivalent Reflectance

Because a detected reflectance change signal is superimposed on the noise of the detecting instru-

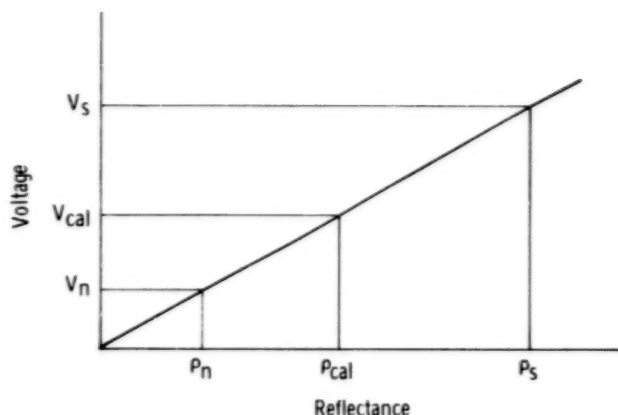


FIGURE 2.—Diagram of system linear in reflectance.

ment, it can be appreciated that the minimum detectable reflectance must create an output signal at least equal to the system noise. In fact, by definition, the resolution of the measuring instrument is that amount of input which produces a signal that is just equal to the noise. Normally, the negligibility of such an input value prevents its convenient use and the measurement task is accomplished (with a linear system, fig. 2) by using a much larger input value and dividing by the signal-to-noise ratio.

$$NE \Delta \rho = \frac{\Delta \rho}{\left(\frac{V_s}{V_n} \right)} \quad (14)$$

where $\Delta \rho$ is the change in scene reflectance required to produce a signal voltage of V_s and V_n is the noise voltage. Thus, $NE \Delta \rho$ is the resolution of the system in terms of reflectance and is the minimum detectable change.

Relationship of NER to $NE \Delta \rho$

From equation (14), it can be seen that $NE \Delta \rho$ depends on the change in reflectance and not on the absolute value of reflectance. On the other hand, the radiance as seen by the scanner (eq. (11)) will depend on both ρ and wavelength λ . To denote the dependence of radiance on wavelength, the notation N_{λ} , which is called spectral radiance and is the partial derivative of radiance with respect to wavelength, is used. To develop an expression for the relationship between spectral radiance and the combination of ρ and λ , a linear approximation may be used for $N_{\lambda}(\rho, \lambda)$ about some values ρ_0, λ_0 ,

where the change in spectral radiance is denoted as ΔN_λ .

$$\Delta N_\lambda \approx \frac{\partial N_\lambda}{\partial \rho} \Delta \rho + \frac{\partial N_\lambda}{\partial \lambda} \Delta \lambda \quad (15)$$

where

$$\Delta N_\lambda = N_\lambda(\rho, \lambda) - N_\lambda(\rho_0, \lambda_0)$$

Dividing each side of equation (15) by the signal-to-noise ratio produces the spectral noise equivalent radiance (NER_λ).

$$\begin{aligned} \frac{\Delta N_\lambda}{S/N} &= NER_\lambda \\ &\approx \frac{\partial N_\lambda}{\partial \rho} \frac{\Delta \rho}{S/N} + \frac{\partial N_\lambda}{\partial \lambda} \frac{\Delta \lambda}{S/N} \end{aligned} \quad (16)$$

The scene or target spectral radiance N_λ can be related to the ground irradiance $H_{g\lambda}$ (ref. 3) by

$$N_{t\lambda} = \frac{\rho}{\pi} [H_{g\lambda} \cos \theta_0 + S_\lambda] + N_{r\lambda} \quad (17)$$

where S_λ is the diffuse or sky irradiance and $N_{r\lambda}$ is the path radiance due to scattering of radiation into the beam from surrounding ground targets. Taking the partial derivatives of equation (17) with respect to ρ and λ results in

$$\frac{\partial N_{t\lambda}}{\partial \rho} = \frac{1}{\pi} [H_{g\lambda} \cos \theta_0 + S_\lambda] \quad (18)$$

$$\frac{\partial N_{t\lambda}}{\partial \lambda} = \frac{\rho}{\pi} \frac{\partial S_\lambda}{\partial \lambda} + \frac{\partial N_{r\lambda}}{\partial \lambda} \quad (19)$$

As a first approximation, it is assumed that

$$\frac{\partial S_\lambda}{\partial \lambda} = 0; \quad \frac{\partial H_{g\lambda}}{\partial \lambda} = 0; \quad \frac{\partial N_{r\lambda}}{\partial \lambda} = 0$$

These approximations are defended on the basis that the variation in the given quantities is small with respect to wavelength. Then, substituting equations (18) and (19) into equation (16), noting that $\Delta \rho / (S/N) = NE \Delta \rho$,

$$NER_\lambda = \frac{NE \Delta \rho}{\pi} [H_{g\lambda} \cos \theta_0 + S_\lambda] \quad (20)$$

Integrating equation (20) with respect to λ results in

$$NER = \frac{NE \Delta \rho}{\pi} \left[\int_{\lambda_1}^{\lambda_2} H_{g\lambda} \cos \theta_0 d\lambda + \int_{\lambda_1}^{\lambda_2} S_\lambda d\lambda \right] \quad (21)$$

Then, if the factor in brackets in equation (21) is denoted as H_t , the total target irradiance, one has

$$NER = \frac{1}{\pi} H_t \cdot NE \Delta \rho \quad (22)$$

Equation (22) is a very useful relationship in determining $NE \Delta \rho$.

Determination of $NE \Delta \rho$

Several means of determining $NE \Delta \rho$ for a scanner system are available; three methods are discussed in the following paragraphs. The first of these is the most direct approach to measurement; it is based on the assumption of a linear system and involves the scanning of two targets of known reflectance.

$$NE \Delta \rho = \frac{\rho_2 - \rho_1}{\left(\frac{V_2 - V_1}{V_n} \right)} \quad (23)$$

where V_1 and V_2 are the output voltages produced by the scanner when aimed at targets 1 and 2, and V_n is the noise voltage of the system. Note that equation (23) is equivalent to equation (14).

A second means of calculating $NE \Delta \rho$ can be derived from equation (13). With the realization that the two variables are the radiance N_λ and the reflectance ρ , write

$$\Delta N_\lambda = \frac{\Delta \rho}{\pi} H_\lambda \cos \theta_0$$

where the deltas represent changes in the quantities. Dividing by S/N ,

$$\begin{aligned} \frac{\Delta N_\lambda}{S/N} &= NER_\lambda \\ &= \frac{\Delta \rho}{S/N} \cdot \frac{H_\lambda \cos \theta_0}{\pi} \\ &= NE \Delta \rho \cdot \frac{H_\lambda \cos \theta_0}{\pi} \end{aligned}$$

Rearranging,

$$NE \Delta\rho = \frac{\pi \cdot NER_{\lambda}}{H_{\lambda} \cos \theta_0} \quad (24)$$

It can be seen that using equation (24) requires that H_{λ} , the solar irradiance, must be known through measurement or calculation or through assumptions involving longitude, atmospheric scattering, transmission, time of day, etc.

The third method of determining $NE \Delta\rho$ is a real-time measurement that uses the internal calibration source of the scanner and a fictitious (but hopefully realistic) solar irradiance value. The method involves a computation of the equivalent reflectance of the internal calibration source.¹

$$NE \Delta\rho = \frac{\rho_{eq}}{\left(\frac{V_{cal}}{V_n}\right)} \quad (25)$$

where ρ_{eq} is equivalent scene reflectance. In this expression, the energy from the calibration lamp is treated as though it were an input from a ground target caused by an external energy source, such as the Sun. To have physical significance, ρ_{eq} obviously must represent a ratio (of energy reflected to energy incident) after the manner of equation (4). Substituting equations (10) and (12) into equation (4),

$$\rho_{eq} = \frac{\pi N_{\lambda}(\text{cal})}{H_{\lambda} \cos \theta_0} \quad (26)$$

where $N_{\lambda}(\text{cal})$ is the calibration source spectral radiance and H_{λ} is an assumed target irradiance produced by incident solar radiation; H_{λ} is the irradiance that would produce a signal N_{cal} after reflection from a fictitious target of reflectivity ρ_{eq} . Thus, the usefulness of $NE \Delta\rho$ as a sensitivity parameter as determined by equation (25) with the use of equation (26) is strongly dependent on the degree to which H_{λ} approximates a true or realistic operational condition. In the JSC Engineering and Development Directorate, a nadir angle of 45° is assumed and H_{λ} is taken from a table compiled by P. Moon (table I) in which a relative air mass of

2.00, an atmospheric pressure of 101.3 kN/m^2 (760 torr), and a water-vapor pressure of 2.7 kN/m^2 (20 torr) are assumed with no provisions for sky or diffuse irradiance. These assumptions bring the measured and calculated numbers into fair agreement. Combining equations (25) and (26), one has

$$NE \Delta\rho = \frac{\pi N_{\lambda}(\text{cal})}{0.707 H_{\lambda}} \cdot \frac{1}{S/N} \\ = \frac{\pi \cdot NER_{\lambda}}{0.707 H_{\lambda}} \quad (27)$$

As calculated from equation (27), $NE \Delta\rho$ is designated as the P. Moon value, the one most used at JSC for the determination of $NE \Delta\rho$ for any particular scanner. To calculate $NE \Delta\rho$ from equation (27), a numerical integration must be performed and this removes the subscript from the two terms.

$$NE \Delta\rho = \frac{\pi \cdot NER}{0.707 H_{\lambda} \Delta\lambda} \\ = \frac{\pi \cdot NER}{0.707 H_p} \quad (28)$$

To illustrate the use of equation (28), $NE \Delta\rho$ will be calculated for the data of September 25, 1975, for channel 2 of the modular multispectral scanner (M²S), the scanner used to acquire the data for this project. The following table will make the procedure more easily understood.

Item	Value	Source
NER	$4.4 \times 10^{-6} \text{ W} \cdot \text{cm}^{-2} \cdot \text{sr}^{-1}$	Table II
Center wavelength	0.465 micrometer	Table III
Bandwidth	0.03 micrometer	Table III
Solar irradiance (P. Moon)	$0.1110 \text{ W} \cdot \text{cm}^{-2} \cdot \mu\text{m}^{-1}$	Table I

Then,

$$NE \Delta\rho = \frac{\pi \times 4.4 \times 10^{-6}}{0.707 \times 0.1110 \times 0.03} \\ = 5.86 \times 10^{-3}$$

and, expressed as a percentage, $NE \Delta\rho$ for channel 2 of the M²S on September 25, 1975, was 0.59 percent. (Other $NE \Delta\rho$ values are listed in table IV.)

¹F. Fulton, Data Processing Requirements for Engineering Evaluation of Bendix MSDS, Lockheed Electronics Company, July 1971.

TABLE I.—Solar Irradiance at Sea Level on an Area Normal to the Sun^a

$$[m = 2; H_0 = 1322 \text{ W} \cdot \text{m}^{-2}]$$

$\lambda, \mu\text{m}$	$H_{\Delta\lambda},$ $\text{W} \cdot \text{m}^{-2} \cdot \mu\text{m}^{-1}$	$\lambda, \mu\text{m}$	$H_{\Delta\lambda},$ $\text{W} \cdot \text{m}^{-2} \cdot \mu\text{m}^{-1}$	$\lambda, \mu\text{m}$	$H_{\Delta\lambda},$ $\text{W} \cdot \text{m}^{-2} \cdot \mu\text{m}^{-1}$	$\lambda, \mu\text{m}$	$H_{\Delta\lambda},$ $\text{W} \cdot \text{m}^{-2} \cdot \mu\text{m}^{-1}$
0.301	0.177	0.68	1149	1.23	420	1.78	18.4
.302	.342	.69	978	1.24	387	1.79	5.70
.303	.647	.70	1108	1.25	328	1.80	.920
.304	1.16	.71	1070	1.26	311	1.81	—
.305	1.91	.72	832	1.27	381	1.82	—
.306	2.89	.73	965	1.28	382	1.83	—
.307	4.15	.74	1041	1.29	346	1.84	—
.308	6.11	.75	867	1.30	264	1.85	—
.309	8.38	.76	566	1.31	208	1.86	—
.310	11.0	.77	968	1.32	168	1.87	—
.311	13.9	.78	907	1.33	115	1.88	—
.312	17.2	.79	923	1.34	58.1	1.89	—
.313	21.0	.80	857	1.35	18.1	1.90	—
.314	25.4	.81	698	1.36	.660	1.91	.705
.315	30.0	.82	801	1.37	—	1.92	2.34
.316	34.8	.83	863	1.38	—	1.93	3.68
.317	39.8	.84	858	1.39	—	1.94	5.30
.318	44.9	.85	839	1.40	—	1.95	17.7
.319	49.5	.86	813	1.41	1.91	1.96	31.7
.32	54.0	.87	798	1.42	3.72	1.97	37.7
.33	101	.88	614	1.43	7.53	1.98	22.6
.34	151	.89	517	1.44	13.7	1.99	1.58
.35	188	.90	480	1.45	23.8	2.00	2.66
.36	233	.91	375	1.46	30.5	2.01	19.5
.37	279	.92	258	1.47	45.1	2.02	47.6
.38	336	.93	169	1.48	83.7	2.03	55.4
.39	397	.94	278	1.49	128	2.04	54.7
.40	470	.95	487	1.50	157	2.05	38.3
.41	672	.96	584	1.51	187	2.06	56.2
.42	733	.97	633	1.52	209	2.07	77.0
.43	787	.98	645	1.53	217	2.08	88.0
.44	911	.99	643	1.54	226	2.09	86.8
.45	1006	1.00	630	1.55	221	2.10	85.6
.46	1080	1.01	620	1.56	217	2.11	84.4
.47	1138	1.02	610	1.57	213	2.12	83.2
.48	1183	1.03	601	1.58	209	2.13	20.7
.49	1210	1.04	592	1.59	205	2.14	—
.50	1215	1.05	551	1.60	202		
.51	1206	1.06	526	1.61	198		
.52	1199	1.07	519	1.62	194		
.53	1188	1.08	512	1.63	189		
.54	1198	1.09	514	1.64	184		
.55	1190	1.10	252	1.65	173		
.56	1182	1.11	126	1.66	163		
.57	1178	1.12	69.9	1.67	159		
.58	1168	1.13	98.3	1.68	145		
.59	1161	1.14	164	1.69	139		
.60	1167	1.15	216	1.70	132		
.61	1168	1.16	271	1.71	124		
.62	1165	1.17	328	1.72	115		
.63	1176	1.18	346	1.73	105		
.64	1175	1.19	344	1.74	97.1		
.65	1173	1.20	373	1.75	80.2		
.66	1166	1.21	402	1.76	58.9		
.67	1160	1.22	431	1.77	38.8		

^aFrom reference 4. See appendix B for definition of symbols.

TABLE II.—Noise Equivalent Radiance

[Watts per square centimeter per steradian]

Channel	Group I	Group II	Group III	Group IV
1	—	22.4×10^{-8}	12.9×10^{-8}	13.7×10^{-8}
2	4.6×10^{-8}	7.1	—	4.7
3	4.1	5.01	4.36	3.70
4	4.1	4.1	3.55	4.20
5	—	3.3	3.7	3.9
6	4.0	3.6	3.6	4.1
7	3.7	4.3	3.6	3.8
8	3.4	6.7	3.4	3.0
9	4.1	11.0	3.3	7.7
10	4.4	7.7	8.09	11.43

TABLE III.—M²S Bandwidths

[Micrometers]

Channel	Band pass	Bandwidth	Center wavelength
1	0.41 to 0.44	0.03	0.425
2	0.45 to 0.48	.03	.465
3	0.49 to 0.53	.04	.51
4	0.53 to 0.57	.04	.55
5	0.57 to 0.61	.04	.59
6	0.61 to 0.65	.04	.63
7	0.65 to 0.69	.04	.67
8	0.69 to 0.74	.05	.71
9	0.76 to 0.86	.10	.81
10	0.95 to 1.03	.08	.99
11	7.89 to 11.64	3.75	9.77

Atmospheric Influence

Equation (22) shows the relationship of NE $\Delta\rho$ to the scene irradiance and the scanner characteristic, NER. To make use of this relationship, one must be able to predict or calculate H_i with some degree of accuracy, and it is here one must consider the effect of the atmosphere. Several atmospheric models are available; one is attributable to Ångström (ref. 5) and has the following form.

$$H_{\lambda} = \cos \theta_0 H_{ex} e^{-m(a_R + a_a) - a_w} + S_{\lambda} \quad (29)$$

where θ_0 is the zenith Sun angle, H_{ex} is the extraterrestrial spectral irradiance (from Thekaekara, table V), and m is air mass and is equal to secant θ for angles between 0° and 60° . The other terms are

TABLE IV.—Tabulation of NE $\Delta\rho$

[Percent]

Channel	Group I	Group II	Group III	Group IV
Measured value				
1	—	1.65	0.74	0.68
2	0.50	.40	—	.19
3	.41	.34	.16	.16
4	.49	.27	.27	.21
5	—	.27	.27	.23
6	.51	.32	.25	.23
7	.53	.33	.25	.21
8	.55	.36	.24	.18
9	.39	.37	.16	.36
10	.66	.55	2.30	3.25
P. Moon value				
1	—	4.37	2.51	2.67
2	0.59	.95	—	.63
3	.38	.46	.40	.34
4	.38	.38	.33	.39
5	—	.32	.35	.37
6	.38	.34	.34	.39
7	.35	.41	.34	.36
8	.28	.55	.28	.25
9	.26	.70	.21	.49
10	.38	.67	.70	.99
Ångström value				
1	—	1.57	0.94	1.00
2	0.31	.39	—	.26
3	.20	.21	.19	.16
4	.23	.18	.16	.19
5	—	.15	.17	.18
6	.24	.17	.18	.20
7	.25	.23	.19	.21
8	.20	.31	.16	.15
9	.16	.34	.11	.25
10	.34	.45	.51	.71
Nomograph value				
1	—	3.88	0.80	0.85
2	0.62	.87	—	.24
3	.38	.44	.17	.14
4	.39	.35	.15	.18
5	—	.27	.15	.16
6	.38	.31	.16	.18
7	.36	.38	.17	.18
8	.29	.50	.14	.13
9	.21	.51	.09	.20
10	.41	.60	.38	.53

TABLE V.—Solar Spectral Irradiance—Proposed Standard Curve^a[Solar constant = 1353 W · m⁻²]

$\lambda, \mu m$	$E(\lambda),$ $W \cdot m^{-2} \cdot \mu m^{-1}$	$E(0-\lambda),$ $W \cdot m^{-2}$	$D(0-\lambda),$ percent	$\lambda, \mu m$	$E(\lambda),$ $W \cdot m^{-2} \cdot \mu m^{-1}$	$E(0-\lambda),$ $W \cdot m^{-2}$	$D(0-\lambda),$ percent
0.120	0.100	0.0059992	0.00044	0.375	1157	89.0641	6.582
.140	.030	.0072993	.00053	.380	1120	94.7566	7.003
.150	.07	.00780	.00057	.385	1098	100.3016	7.413
.160	.23	.00930	.00068	.390	1098	105.7916	7.819
.170	.63	.01360	.00100	.395	1189	111.5091	8.241
.180	1.25	.02300	.00169	.400	1429	118.0541	8.725
.190	2.71	.04280	.00316	.405	1644	125.7366	9.293
.200	10.7	.10985	.00811	.410	1751	134.2241	9.920
.210	22.9	.27785	.02053	.415	1774	143.0366	10.571
.220	57.5	.67985	.05024	.420	1747	151.8391	11.222
.225	64.9	.98585	.0728	.425	1693	160.4391	11.858
.230	66.7	1.31485	.0971	.430	1539	168.7691	12.473
.235	59.3	1.62985	.1204	.435	1563	177.0241	13.083
.240	63.0	1.93560	.1430	.440	1810	185.7066	13.725
.245	72.3	2.27385	.1680	.445	1922	195.0356	14.415
.250	70.4	2.63060	.1944	.450	2006	204.8566	15.140
.255	104	3.06660	.2266	.455	2057	215.0141	15.891
.260	130	3.65160	.2698	.460	2066	225.3216	16.653
.265	165	4.43910	.3280	.465	2049	235.6066	17.413
.270	232	5.48160	.4051	.470	2033	245.8091	18.167
.275	204	6.5716	.4857	.475	2044	256.001	18.921
.280	222	7.6366	.5644	.480	2074	266.296	19.681
.285	315	8.9791	.6636	.485	1976	276.421	20.430
.290	482	10.9716	.8109	.490	1950	286.236	21.155
.295	584	13.6366	1.0078	.495	1960	296.011	21.878
.300	514	16.3816	1.2107	.500	1942	305.766	22.599
.305	603	19.1741	1.4171	.505	1923	315.421	23.312
.310	689	22.4041	1.6558	.510	1982	324.926	24.015
.315	764	26.0366	1.9243	.515	1933	334.214	24.701
.320	830	30.0216	2.2188	.520	1933	343.379	25.379
.325	975	34.5341	2.552	.525	1852	352.591	26.059
.330	1059	39.6191	2.928	.530	1842	361.826	26.742
.335	1081	44.9691	3.323	.535	1819	370.976	27.418
.340	1074	50.3566	3.721	.540	1783	379.979	28.084
.345	1069	55.7141	4.117	.545	1754	388.821	28.737
.350	1093	61.1191	4.517	.550	1725	397.519	29.380
.355	1083	66.5591	4.919	.555	1720	406.131	30.017
.360	1068	71.9366	5.316	.560	1695	414.669	30.648
.365	1132	77.4366	5.723	.565	1705	423.169	31.276
.370	1181	83.2191	6.150	.570	1712	431.711	31.907

^aFrom reference 6. See appendix B for definition of symbols.

given in appendix B but some discussion is in order. The quantity a_R is the Rayleigh extinction coefficient (or scattering coefficient) and it provides a measure of the reflective interaction between the solar radiant energy and the molecules of

the gaseous atmosphere. This coefficient is wavelength dependent and is given by

$$a_R(\lambda) = 0.00889\lambda^{-4.05} \quad (30)$$

TABLE V.—Continued

$\lambda, \mu m$	$E(\lambda),$ $W \cdot m^{-2} \cdot \mu m^{-1}$	$E(0-\lambda),$ $W \cdot m^{-2}$	$D(0-\lambda),$ percent	$\lambda, \mu m$	$E(\lambda),$ $W \cdot m^{-2} \cdot \mu m^{-1}$	$E(0-\lambda),$ $W \cdot m^{-2}$	$D(0-\lambda),$ percent
0.575	1719	440.289	32.541	0.94	847	892.08	65.934
.580	1715	448.874	33.176	.95	837	900.50	66.556
.585	1712	457.441	33.809	.96	820	908.79	67.168
.590	1700	465.971	34.439	.97	803	916.90	67.768
.595	1682	474.426	35.064	.98	785	924.84	68.355
.600	1666	482.796	35.683	.99	767	932.60	68.928
.605	1647	491.079	36.295	1.00	748	940.18	69.488
.610	1635	499.284	36.902	1.05	668	975.58	72.105
.620	1602	515.469	38.098	1.10	593	1007.10	74.435
.630	1570	531.329	39.270	1.15	535	1035.30	76.519
.64	1544	546.899	40.421	1.20	485	1060.80	78.404
.65	1511	562.174	41.550	1.25	438	1083.88	80.101
.66	1486	577.159	42.557	1.30	397	1104.75	81.652
.67	1456	591.869	43.744	1.35	358	1123.63	83.047
.68	1427	606.284	44.810	1.40	337	1141.00	84.331
.69	1402	620.429	45.855	1.45	312	1157.23	85.530
.70	1369	634.284	46.879	1.50	288	1172.23	86.639
.71	1344	647.849	47.882	1.55	267	1186.10	87.665
.72	1314	661.139	48.864	1.60	245	1198.40	88.611
.73	1290	674.159	49.826	1.65	223	1210.60	89.475
.74	1260	686.909	50.769	1.70	202	1221.23	90.261
.75	1235	699.384	51.691	1.75	180	1230.78	90.967
.76	1211	711.614	52.595	1.80	159	1239.25	91.593
.77	1185	723.594	53.480	1.85	142	1246.78	92.149
.78	1159	735.314	54.346	1.90	126	1253.48	92.644
.79	1134	746.779	55.194	1.95	114	1259.48	93.088
.80	1109	757.994	56.023	2.00	103	1264.90	93.489
.81	1085	768.966	56.834	2.10	90	1274.55	94.202
.82	1060	779.694	57.627	2.20	79	1283.00	94.826
.83	1036	790.174	58.401	2.30	69	1290.40	95.373
.84	1013	800.419	59.158	2.4	62.0	1296.95	95.8580
.85	990	810.434	59.899	2.5	55.0	1302.80	96.2903
.86	968	820.224	60.622	2.6	48.0	1307.95	96.6710
.87	947	829.793	61.330	2.7	43.0	1312.50	97.0073
.88	926	839.164	62.022	2.8	39.0	1316.60	97.3103
.89	908	848.334	62.700	2.9	35.0	1320.30	97.5838
.90	891	857.329	63.365	3.0	31.0	1323.60	97.8277
.91	880	866.184	64.019	3.1	26.0	1326.45	98.0383
.92	869	874.929	64.665	3.2	22.6	1328.88	98.2179
.93	858	883.564	65.304	3.3	19.2	1330.97	98.3724

where λ is given in micrometers. The quantity a_a is an aerosol attenuation coefficient due to dust, haze, etc., and is approximated by

$$a_a(\lambda) = 2.303B(2\lambda)^{-\alpha} \quad (31)$$

which introduces two more quantities, B and α . The term B is called a turbidity constant, the values for which range from 0.05 to 0.2 (table VI); α takes

on a value $0 < \alpha \leq 4$, depending on particle size, and is given the value 1.0 for light haze and the value 1.5 for clear conditions. The quantity a_w is an attenuation coefficient that varies with latitude and wavelength but, for a water-vapor pressure of 2.7 kN/m² (20 torr), is 0.011 for $0.4 \leq \lambda \leq 0.7$ micrometer and 0.18 for $0.6 \leq \lambda \leq 1.0$ micrometer. The quantity S_λ , diffuse sky irradiance, is highly variable but can be approximated from experimen-

TABLE V.—Concluded

$\lambda, \mu m$	$E(\lambda),$ $W \cdot m^{-2} \cdot \mu m^{-1}$	$E(0-\lambda),$ $W \cdot m^{-2}$	$D(0-\lambda),$ percent
3.4	16.6	1332.76	9.5047
3.5	14.6	1334.32	98.1200
3.6	13.5	1335.73	98.1738
3.7	12.3	1337.02	98.892
3.8	11.1	1338.19	98.906
3.9	10.3	1339.26	98.984
4.0	9.5	1340.25	99.057
4.1	8.7	1341.16	99.1252
4.2	7.8	1341.98	99.1861
4.3	7.1	1342.73	99.2412
4.4	6.50	1343.4141	99.291507
4.5	5.90	1344.0341	99.337331
4.6	5.30	1344.5941	99.378721
4.7	4.80	1345.0991	99.416045
4.8	4.50	1345.5641	99.450413
4.9	4.10	1345.9941	99.482195
5.0	3.83	1346.3906	99.511500
6.0	1.75	1349.1806	99.717708
7.0	.99	1350.5506	99.818965
8.0	.60	1351.3456	99.877723
9.0	.380	1351.8356	99.913939
10.0	.250	1352.1506	99.937221
11.0	.170	1352.3606	99.952742
12.0	.120	1352.5056	99.963459
13.0	.087	1352.6091	99.971108
14.0	.055	1352.6801	99.976356
15.0	.049	1352.7321	99.980199
16.0	.038	1352.7756	99.983414
17.0	.031	1352.8101	99.985964
18.0	.024	1352.8376	99.987997
19.0	.02000	1352.8526	99.985623
20.0	.01600	1352.8776	99.990953
25.0	.00610	1352.9228	99.995037
30.0	.00300	1352.9556	99.996718
35.0	.00160	1352.9671	99.997568
40.0	.00094	1352.9734	99.998037
50.0	.00032	1352.9800	99.998525
60.0	.00019	1352.9829	99.998736
80.0	.00007	1352.9855	99.998928
100.0	.00001	1352.9865	99.999002
1000.0	.00000	1353.0000	100.000000

tal evidence which shows that $S_\lambda/H_\lambda \approx 0.35$ for wavelengths between 0.4 and 0.6 micrometer, and $S_\lambda/H_\lambda \approx 0.1$ for wavelengths between 0.6 and 1.0 micrometer (ref. 5).

The wavelength dependency of the exponents in equation (29) results in a formidable expression. However, simplifications are possible in a measure-

TABLE VI.—Standard Values of the Turbidity Coefficient B as a Function of Latitude and Altitude

Altitude (air pressure), kNm^2 (mbar)	Level	Latitude							
		70° N	60° N	45° N	30° N	0°	30° S	45° S	60° S
100 (1000)	Ångström	0.050	0.061	0.082	0.104	0.125	0.104	0.082	0.061
	Lower limit	.010	.010	.050	.050	.050	.050	.050	.010
	Upper limit	.100	.100	.200	.400	.400	.400	.200	.100
90 (900)	Ångström	.030	.037	.050	.063	.076	.063	.050	.037
	Lower limit	.010	.010	.010	.010	.010	.010	.010	.010
	Upper limit	.050	.100	.100	.200	.400	.200	.100	.050
80 (800)	Ångström	.018	.022	.030	.037	.046	.037	.030	.022
	Lower limit	.000	.000	.010	.010	.010	.010	.010	.000
	Upper limit	.050	.050	.100	.200	.200	.200	.100	.050
70 (700)	Ångström	.011	.014	.018	.023	.028	.023	.018	.014
	Lower limit	.000	.000	.000	.010	.010	.010	.000	.000
	Upper limit	.020	.050	.050	.100	.200	.100	.050	.050

ment situation because the relatively narrow bands used in a scanner system permit the use of approximations within a band. Thus, to find the scene irradiance in a band corresponding to the detector responses, an integration of equation (29) would be performed in the following way.

$$\int_{\lambda_1}^{\lambda_2} H_\lambda d\lambda = H_b$$

$$= \left\{ \cos \theta_0 e^{-m[a_R(\lambda_c) + a_a(\lambda_c)] - a_w(\lambda_c)} \right\} \cdot H_{eb} + S_b \quad (32)$$

where

$$H_{eb} = \int_{\lambda_1}^{\lambda_2} H_{ex} d\lambda$$

and

$$S_b = \int_{\lambda_1}^{\lambda_2} S_\lambda d\lambda$$

and the (λ_c) 's are the center wavelengths of the band passes. Finally, NE $\Delta\rho$ is computed for a given scanner and considering the atmospheric attenuation.

$$NE \Delta\rho = \frac{\pi \cdot NE R}{H_b} \quad (33)$$

where H_b is the value taken from equation (32). Another atmospheric model, which deals with the terms optical depth and visibility, is discussed in the following paragraphs and in appendix A.

To illustrate the use of equations (32) and (33), NE $\Delta\rho$ will be computed using M²S data acquired on May 15, 1978. The method is best illustrated using the following table.

Item	Value	Source
θ	26.06°	Table VII
$\cos \theta$	0.90	Computation
m	1.11	$m = \secant \theta$
λ_c	0.55 micrometer	Table III (channel 4)
a_R	0.10	$a_R = 0.00889\lambda^{-4.05}$
B	0.082	Table VI, latitude 45°
α	1.5	Assumption
a_a	0.16	$a_a = 2.303B(2\lambda)^{-\alpha}$
a_w	0.011	Text
$\Delta\lambda$	0.04 micrometer	Table III (channel 4)
H_λ	$1725 \times 10^{-4} \text{ W} \cdot \text{cm}^{-2} \cdot \mu\text{m}^{-1}$	Table V (0.55 micrometer)
S_b	$2.28 \times 10^{-2} \text{ W} \cdot \text{cm}^{-2}$	Text
NER	$3.55 \times 10^{-6} \text{ W} \cdot \text{cm}^{-2} \cdot \text{sr}^{-1}$	Table II

According to Robinson (ref. 5), S is approximated from experimental evidence which shows that $S_\lambda/H_\lambda \approx 0.35$ for wavelengths between 0.4 and 0.6 micrometer and $S_\lambda/H_\lambda \approx 0.1$ for wavelengths between 0.6 and 1.0 micrometer. A curve is drawn (fig. 3) to approximate this condition and remove the discontinuity. The 0.55-micrometer band

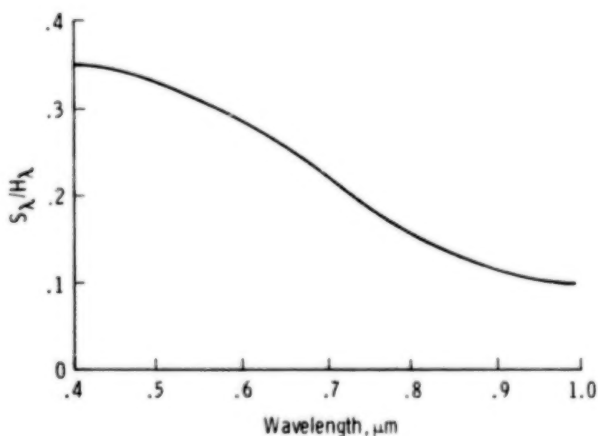


FIGURE 3.—Ratio of diffuse irradiance to solar irradiance as a function of wavelength.

(channel 4) then has a value of 0.33 for S_λ/H_λ . Then,

$$\begin{aligned} S_\lambda &= H_\lambda \times 0.33 \\ &= 1725 \times 10^{-4} \times 0.33 \\ &= 5.69 \times 10^{-2} \end{aligned}$$

and

$$\begin{aligned} S_b &= \int S_\lambda d\lambda \approx S_\lambda \Delta\lambda \\ &= 5.69 \times 10^{-2} \Delta\lambda \\ &= 2.28 \times 10^{-3} \end{aligned}$$

Then, from equation (32),

$$\begin{aligned} H_b &= [0.90e^{-1.11(0.1+0.16)-0.011}] 1725 \times 10^{-4} (0.04) \\ &\quad + 2.28 \times 10^{-3} \\ &= 6.88 \times 10^{-3} \end{aligned}$$

Then, substituting into equation (33),

$$\begin{aligned} \text{NE } \Delta\rho &= \frac{\pi \cdot \text{NER}}{H_b} \\ &= \frac{\pi \times 3.55 \times 10^{-6}}{6.88 \times 10^{-3}} \\ &= 0.16 \text{ percent} \end{aligned}$$

Other values of Ångström's NE $\Delta\rho$ are given in table IV.

Assuming that the Ångström or any other model describes at least the average properties of the atmosphere, it is possible to develop a range of values for NE $\Delta\rho$ under given atmospheric conditions; and atmospheric conditions are best described, in a practical sense, in terms of visibility or visual range. Visual range is related to aerosol or haze scattering and is a quantity quoted by the National Weather Service as a measure of the gross features of atmospheric conditions. These have been classified and correspond to the attenuation of the atmosphere at 0.55 micrometer as haze, clear,

TABLE VII.—Summary of Available Meteorological Data for Flight Dates

Item	Data groups—flight dates			
	Group I— Sept. 25, 1975	Group II— July 8, 1976	Group III— May 15, 1978	Group IV— June 2, 1978
Latitude, deg N	44.563	44.563	44.563	44.563
Longitude, deg W	98.908	98.908	98.908	98.908
Altitude, m (ft)	451 (1480)	451 (1480)	451 (1480)	451 (1480)
Local time	1346	1343	1337	1228
Sun angle, deg	44.50	22.50	26.06	26.96
Solar declination, deg	-0.520139	22.4862	18.7265	22.1083
Relative air mass	1.402	1.082	1.079	1.122
Cloud cover, percent	NA ^a	5	20	0
Relative humidity, percent	NA	30	54	35
Barometric pressure, kN/m ² (in. Hg)	NA	96.17 (28.40)	96.24 (28.42)	96.85 (28.60)
General conditions	NA	Haze, dust	Clear	Clear

^aNot available.

etc. The optical depth of the atmosphere to haze attenuation is then related to visual range, which is the distance R_v at which the ratio of the apparent contrast of an object viewed with background radiation, viewed by an observer at range R , to the inherent contrast at zero range is equal to 2 percent. Figure 4 shows the relationship of the terms "clear," "very clear," "haze," etc., with daylight visibility range in kilometers. Atmospheric models that are used to correct remote-sensing data have been developed which make use of the visual range quantity. One such model, attributable to Turner (ref. 7), has the form

$$H_b = H_e \cos \theta_0 e^{-m(\tau_R + \tau_a)} + S_t \quad (34)$$

There is a great deal of similarity in the appearance of equation (34), Turner's model, and equation (29), Ångström's model. Turner's model does not include a water absorption quantity as does Ångström's model as in the term a_w . Since it is primarily the visible region of the spectrum that is involved, there is no inconsistency because a_w is very small below 0.72 micrometer, and Ångström's model is simply more general. The attractiveness of equation (34) lies in the use which is made of the actual condition, visual range. The exponent in equation (34) introduces the terms τ_R and τ_a , which are the total Rayleigh optical depth (fig. 5) and the aerosol optical depth (fig. 6), respectively. The subscript t is used on the sky irradiance term S_t to

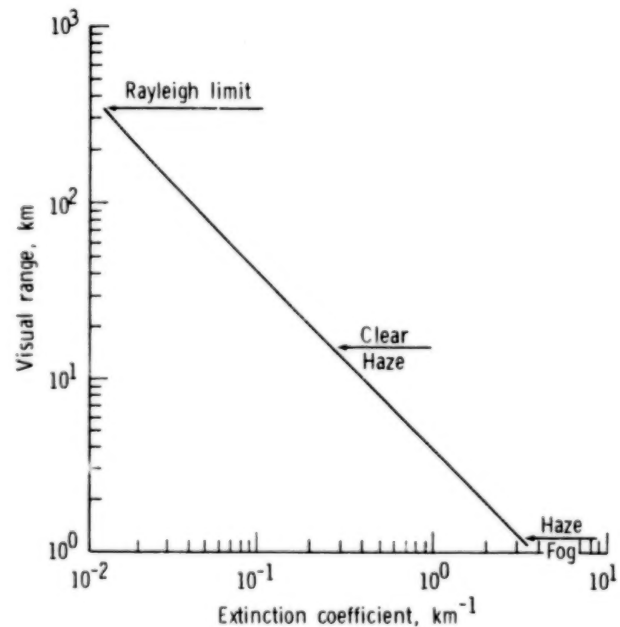


FIGURE 4.—Variation of visual range with extinction coefficient at a wavelength of 0.55 micrometer.

make a distinction from the S_b term in equation (34); S_t is found from the relationship (ref. 7)

$$\begin{aligned} \frac{S_t}{H_b} &= k \cos \theta_0 \\ &= \frac{k}{m} \end{aligned} \quad (35)$$

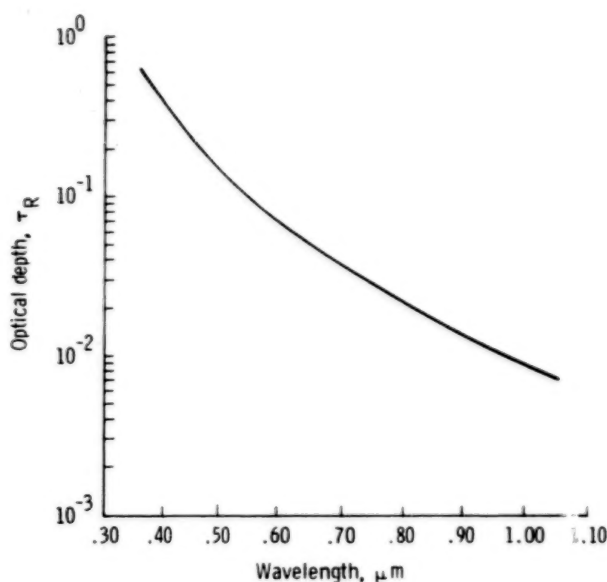


FIGURE 5.—Dependence of total Rayleigh optical depth τ_R on wavelength.

and for the data in this report,

$$k = qm - 0.68 \quad (36)$$

where

$$q = e^{\tau_R + \tau_a} \quad (37)$$

The value 0.68 in equation (36) is an empirically derived constant related primarily to the scanner characteristics. From equation (33),

$$NE \Delta\rho = \frac{\pi}{H_b} NER \quad (33)$$

Using equations (34) and (35), substituting in equation (33), and rearranging terms,

$$\left[\frac{NE \Delta\rho}{NER} \right] \left[\frac{H_b}{\pi} \right] = \frac{mq^m}{\left(\frac{1 + S_t}{H_b} \right)} \quad (38)$$

An inspection reveals that the left side of equation (38) consists of scanner terms and the right side relates to physical conditions, which in turn relate to the latitude of the observation, the time of day, and the state of the atmosphere, etc. With equations (35) and (36), equation (38) becomes

$$\left[\frac{NE \Delta\rho}{NER} \right] \left[\frac{H_e}{\pi} \right] = \frac{mq^m}{\left(1 - \frac{0.68}{m} \right) + q} \quad (39)$$

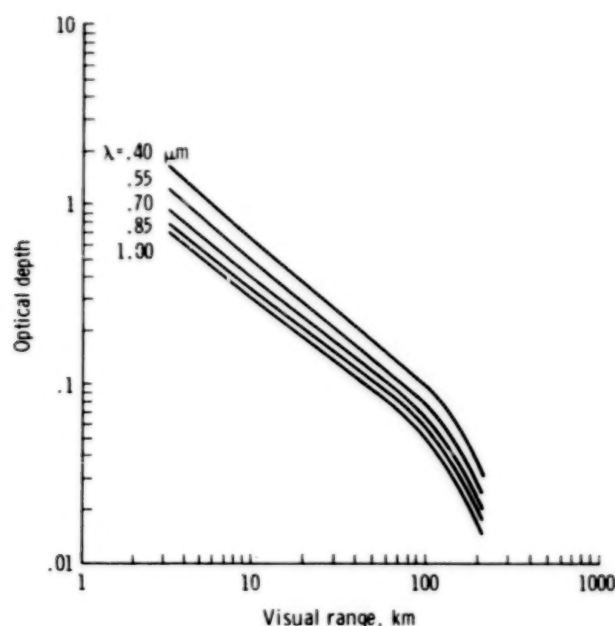


FIGURE 6.—Aerosol optical depth τ_a as a function of visual range R_v . Parameter is spectral wavelength λ in micrometers.

Equation (39) forms the basis of nomographs wherein one may resolve scanner system sensitivity on the basis of the conditions relating to the data situation. The value for m may be calculated or may be taken from the graph in figure 7, which is a plot of air mass as a function of time T in hours before or after noon for two latitudes and three seasons of the year. This value of m is used with figures 8, 9, and 10 to find a value, a unitless number, for the left side of equation (39). Then, knowing the scanner NER and the extraterrestrial irradiance from table V for the center wavelength of a particular scanner band, one may calculate $NE \Delta\rho$. Following is a step-by-step procedure for calculating $NE \Delta\rho$.

1. Using figure 7, estimate the air mass for a given latitude and time of day. The air mass may also be calculated as indicated in appendix A since $m = 1/\cos \theta$.

2. Using figure 4 and an estimate of the visibility conditions, find the daylight visibility range.

3. Using the appropriate figure (8, 9, or 10, correlative to haze, clear, or exceptionally clear) for the ratio of system parameters, estimate the $NE \Delta\rho$ value for that channel given π , H_e , and NER.

As an example, consider the data obtained with the M²S for channel 2 on June 2, 1978: (1) $\lambda_c = 0.47$ micrometer (table III), (2) $\Delta\lambda = 0.03$ micrometer (table III), (3) $NER = 4.7 \times 10^{-6}$

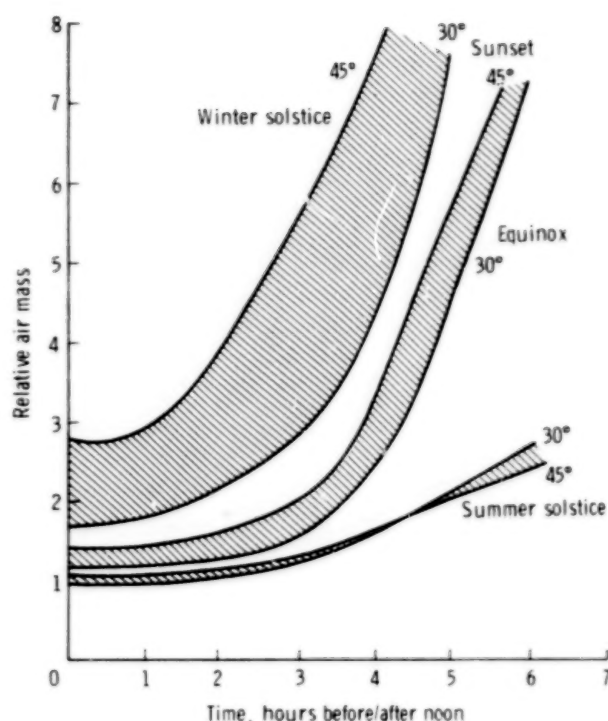


FIGURE 7.—Air mass m as a function of time.

$W \cdot \text{cm}^{-2} \cdot \text{sr}^{-1}$ (table II), (4) $H_e = H_{e\lambda} \Delta\lambda = 2033 \times 10^{-4} \times 0.03 = 6.1 \times 10^{-3}$ (tables III and V), (5) time of day = 12:30 p.m. = 0.5 hour after noon (table VII), (6) latitude = 44.5°N (table VII), and (7) air mass = 1.122 (table VII). From figure 7 for 0.5 hour after noon, an air mass of approximately 1.0 is found. (Summer solstice occurs June 21 or 22.) First, considering a hazy day, a value of 1.1 is obtained for the scanner constants (fig. 8). Thus,

$$\begin{aligned} \text{NE } \Delta\rho &= \frac{\pi \cdot \text{NER} \times 1.1}{H_e} \\ &= \frac{\pi \times 4.7 \times 10^{-6} \times 1.1}{6.1 \times 10^{-3}} \\ &= 0.27 \text{ percent} \end{aligned}$$

The figure 0.27 percent, calculated assuming haze, is the worst condition. Assuming clear conditions (visibility equals 15 kilometers), the best value of 0.23 percent is obtained. This compares with the experimental or measured value of 0.19 percent. Hence, the expected value at this location and time would be about 0.25 percent regardless of the atmospheric state. This constancy is due, of course, to the optimum time of the particular data run.

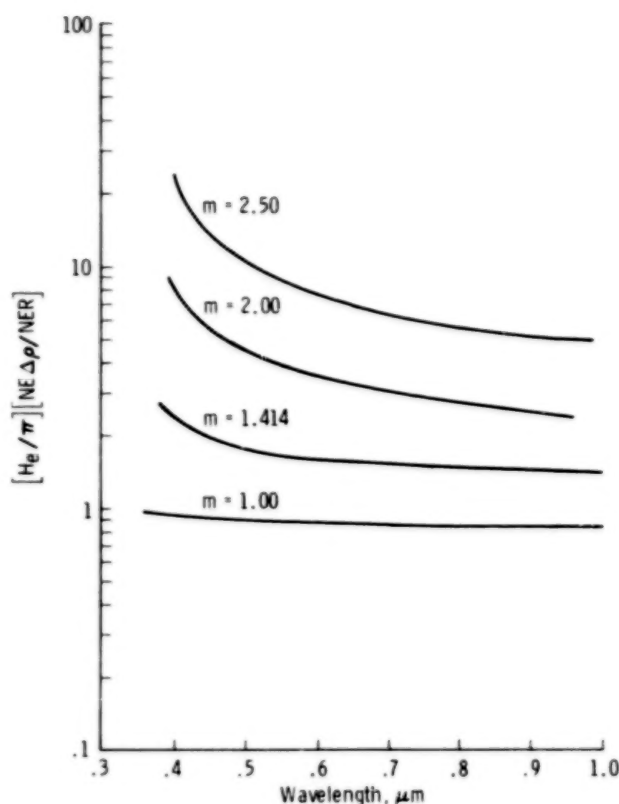


FIGURE 8.—Nomograph of scanner parameters for haze condition; visibility = 4 kilometers.

Direct Measurement of $\text{NE } \Delta\rho$

One of the major activities of the JSC Earth Resources Program is the Large Area Crop Inventory Experiment (LACIE). The LACIE is a long-term project designed to develop remote-sensing techniques for the total assessment of agricultural targets. The LACIE procedure includes the collection of a limited amount of meteorological data and the deployment of ground-truth reflectance panels adjacent to the agricultural targets. These targets are overflown by a multitude of sensor systems including the 11-channel modular multispectral scanner, which generated the data used in this report. The data used were collected over an area in Hand County, South Dakota, situated at 451 meters (1480 feet) above sea level. Flight dates were September 25, 1975; July 8, 1976; May 15, 1978; and June 2, 1978. The data for these dates have been designated as Groups I, II, III, and IV, respectively, where used in the tables. Five reflectance panels with nominal reflectances of 60, 28, 16, 8, and 5 percent (figs. 11 and 12), with dimensions of 6.1 by 12.2 meters (20 by 40 feet), are deployed side by

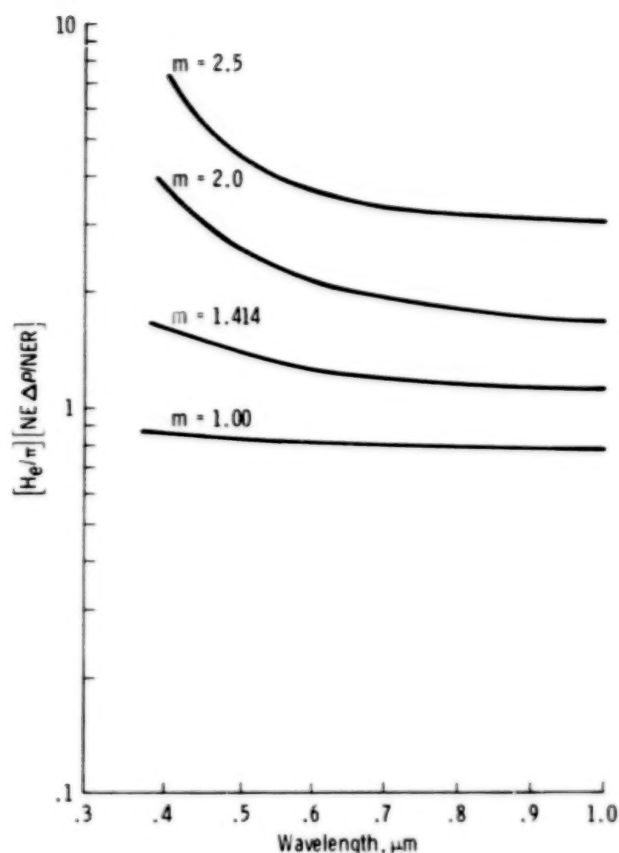


FIGURE 9.—Nomograph of scanner parameters for clear condition; visibility = 15 kilometers.

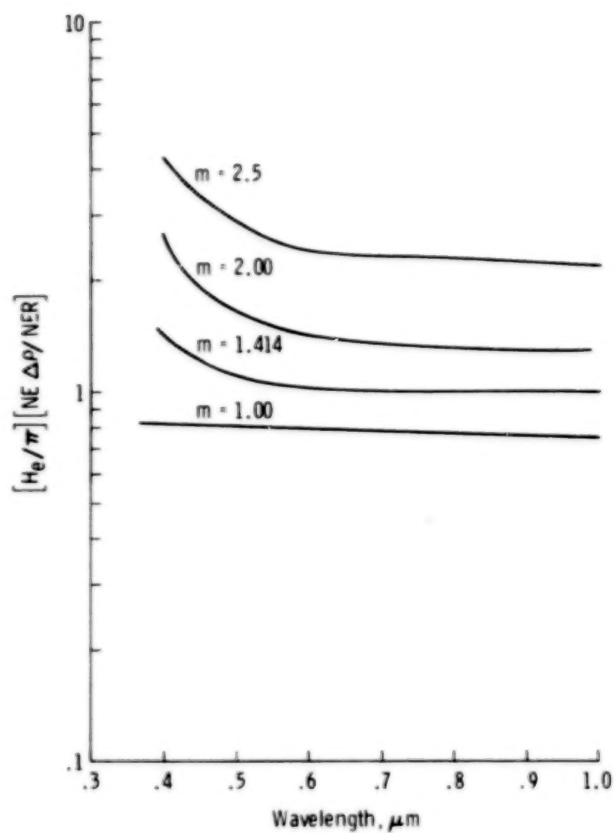


FIGURE 10.—Nomograph of scanner parameters for exceptionally clear condition; visibility = 100 kilometers.

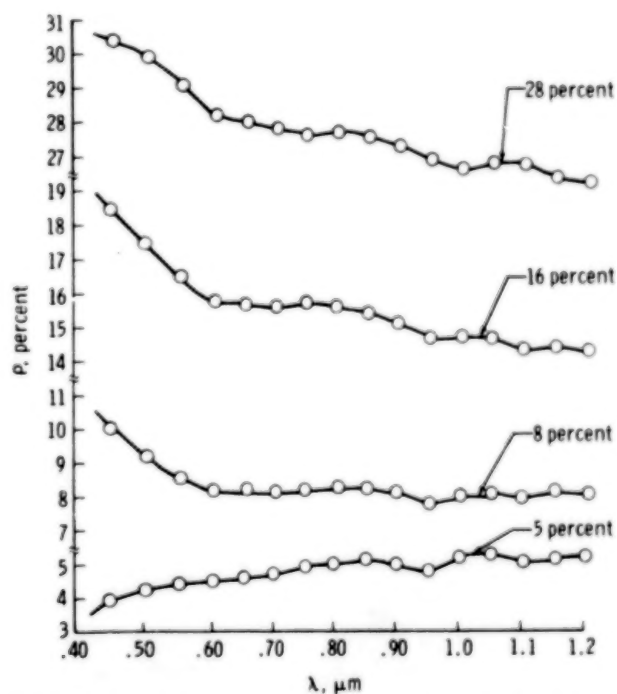


FIGURE 11.—Reflectance as a function of wavelength for 5-, 8-, 16-, and 28-percent-reflectance panels (September 25, 1975).

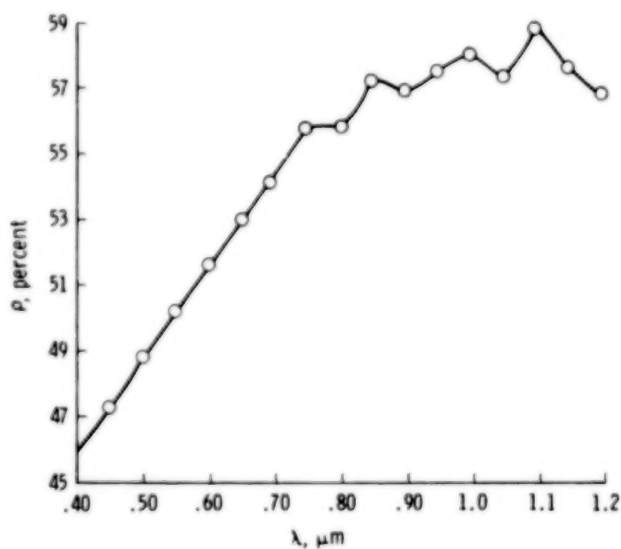


FIGURE 12.—Reflectance as a function of center wavelength for 60-percent-reflectance panel (September 25, 1975).

side. The data collection altitude is 457.2 to 609.6 meters (1500 to 2000 feet), so that, with the 2.5-milliradian instantaneous field of view (IFOV) of the M²S sensor, between 8 and 10 data points (resolution elements or "reselms") are obtained each scan line for 4 or 5 scans as the scanner overflies a panel. Each reselm is digitized into 8 bits and recorded on tape so that the panel data are located in the printout through inspection by finding clusters of similar numbers in a 4 by 8 or a 5 by 10 matrix. (See data in fig. 13.) These matrices are correlated with specific panels by virtue of the correspondence of higher numbers with higher reflectances. When this correlation of signals with reflectance panels has been accomplished, the next step in computing NE $\Delta\rho$ is to obtain a noise figure or signal.

Noise is measured by noting the variations in the system output as the scanner is subjected to a uniform target. A convenient target of 8-reselm size is provided by the internal calibration or reference source, which is viewed once each scan. The noise is considered to be the standard deviation for the scanner output when the calibration source is viewed. Sufficient information is then available, using equation (23), to calculate NE $\Delta\rho$ from direct measurements.

$$NE \Delta\rho = \frac{\rho_2 - \rho_1}{\left(\frac{V_2 - V_1}{V_n} \right)} \quad (23)$$

where ρ_2 and ρ_1 are the reflectances of any two panels, V_2 and V_1 are the corresponding average counts, and V_n is the standard deviation of the counts while the scanner is viewing the calibration source.

Each of the 10 visible channels for the M²S was analyzed by plotting the value of the reflectance of the panel taken at the center of the half-power bandwidths, λ_c , as determined from laboratory calibration reports.^{2,3} By taking the low blackbody reference source as "zero" reflectance, a straight line was obtained as shown in figure 14. If the reflectance change and signal change between each panel are used, the result is a second straight line the slope of which is the same as the first but which

²R. W. Nuss and J. R. Woodfill, Project ERAP Modular Multispectral Scanner Data Evaluation Report, JSC-09257, Oct. 1974.

³D. Hawley, M²S Engineering Baseline and Calibration Test Report, NASA-LEC 4969, 1975.

SENSOR ANALYSIS LABORATORY 4-2140

CESA PROGRAM

9/25/75

RAW DATA CHANNEL	10	ME	317	FLT	27	SC	11100	TO	11200	9	10
1	110	117	120	119	115	113	115	114	112	117	
2	117	120	119	118	110	117	110	117	117	115	
3	119	118	122	118	110	117	119	115	114	117	
4	120	117	110	119	110	119	117	114	113	117	
5	115	115	120	113	115	115	117	117	113	114	
6	110	111	114	117	117	117	117	117	113	117	
7	113	113	115	112	115	115	117	115	110	115	
8	114	117	115	115	113	115	120	110	117	115	
9	114	115	115	115	117	115	120	117	115	119	
10	112	115	117	117	114	113	119	117	119	119	
11	117	117	117	117	117	117	119	110	115	120	
12	117	119	117	117	117	115	110	117	117	121	
13	115	115	114	115	114	112	110	110	125	125	
14	110	114	117	117	115	115	120	110	123	122	
15	113	115	110	120	110	115	117	110	121	123	
16	113	114	117	110	110	115	116	120	123	122	
17	114	117	117	110	112	110	121	125	120	120	
18	117	119	117	117	117	119	120	119	120	119	
19	117	119	117	117	117	119	120	119	120	119	
20	115	115	115	115	115	115	115	115	115	115	
21	114	114	114	114	114	114	114	114	114	114	
22	112	112	112	112	112	112	112	112	112	112	
23	112	112	112	112	112	112	112	112	112	112	
24	115	115	115	115	115	115	115	115	115	115	
25	117	117	117	117	117	117	117	117	117	117	
26	114	117	117	117	117	117	117	117	117	117	
27	114	112	112	112	112	112	112	112	112	112	
28	117	113	113	113	113	113	113	113	113	113	
29	115	111	111	111	111	111	111	111	111	111	
30	114	114	114	114	114	114	114	114	114	114	
31	110	114	114	114	114	114	114	114	114	114	
32	119	114	114	114	114	114	114	114	114	114	
33	113	114	114	114	114	114	114	114	114	114	
34	113	110	110	110	110	110	110	110	110	110	
35	112	110	110	110	110	110	110	110	110	110	
36	112	114	114	114	114	114	114	114	114	114	
37	112	112	114	114	114	114	114	114	114	114	
38	115	110	110	110	110	110	110	110	110	110	
39	111	113	113	113	113	113	113	113	113	113	
40	112	113	113	113	113	113	113	113	113	113	
41	112	111	111	111	111	111	111	111	111	111	
42	111	112	110	110	110	110	110	110	110	110	
43	111	114	114	114	114	114	114	114	114	114	
44	115	114	114	114	114	114	114	114	114	114	
45	117	114	114	114	114	114	114	114	114	114	
46	117	117	117	117	117	117	117	117	117	117	
47	117	117	117	117	117	117	117	117	117	117	
48	112	114	114	114	114	114	114	114	114	114	
49	111	113	113	113	113	113	113	113	113	113	
50	110	110	110	110	110	110	110	110	110	110	
51	111	110	110	110	110	110	110	110	110	110	
52	113	112	110	110	110	110	110	110	110	110	
53	117	114	114	114	114	114	114	114	114	114	
54	112	115	114	114	114	114	114	114	114	114	
55	113	117	117	117	117	117	117	117	117	117	
56	112	115	115	115	115	115	115	115	115	115	
57	117	117	117	117	117	117	117	117	117	117	
58	112	114	114	114	114	114	114	114	114	114	
59	112	115	114	114	114	114	114	114	114	114	
60	111	113	113	113	113	113	113	113	113	113	
61	111	112	112	112	112	112	112	112	112	112	
62	112	112	112	112	112	112	112	112	112	112	
63	112	112	114	114	114	114	114	114	114	114	
64	112	113	113	113	113	113	113	113	113	113	
65	110	110	112	112	112	112	112	112	112	112	

FIGURE 13.—Sample printout of M²S data showing clustering method used for locating reflectance panel data.

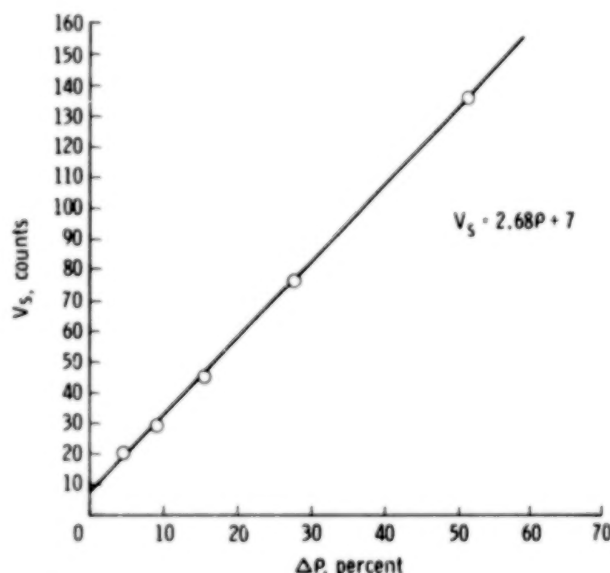


FIGURE 14.—Plot of scene signal voltage as a function of relative reflectance for channel 7 (September 25, 1975).

also passes through the zero signal-to-noise point (fig. 15). The slope of the reflectance as a function of the signal-to-noise ratio is the NE $\Delta\rho$ for the channel.

It would be profitable at this point to discuss why the line passes through zero in one case but not the other. First, it can be seen from the graph in figure 15 that the line not passing through zero can be corrected to zero reflectance by a simple subtraction of a constant offset count. The source of the offset term can be understood by reference to equation (17), which, upon integration over wavelength, provides scene radiance.

$$N_s = \frac{\rho}{\pi} [H_e \cos \theta_0 + S] + N_a \quad (40)$$

In equation (40), note that, for $\rho = 0$ percent, the scene radiance observed by the scanner is equal to the backscatter term N_a . Letting the responsivity of the scanner system be $R = V_s/N_s$, then, in terms of counts,

$$V_s = \frac{\rho}{\pi} [H_{ex} \cos \theta_0 + S] R + V_a \quad (41)$$

A schematic of the signal as a function of time is shown in figure 16, in which V_a represents the zero-offset term. Thus, a panel-to-panel measurement is simpler than a panel-to-zero-radiance measurement because the backscatter term disappears.

Comparison of Measured and Calculated NE $\Delta\rho$

Values of NE $\Delta\rho$ for the data acquired for the four flight dates of September 1975, July 1976, May 1978, and June 1978 are recorded in table IV. Included in this table are the Perry Moon values calculated from equation (28), the Ångström values calculated using equation (33), and the values extracted using the nomograph discussed previously. In the P. Moon values, scene irradiance H is taken from table I, and N_{cal} and S/N are sensor performance parameters taken from laboratory tests. As previously stated, the P. Moon values are calculated assuming an air mass of 2.0, which corresponds to a Sun angle of 60° measured from the zenith. The P. Moon value, then, is a rough calculation meant to produce a sensitivity number with regard to possible, but not necessarily actual, conditions. In the Ångström values, NER is taken from laboratory data, and H_b comes from the use of the Thekaekara

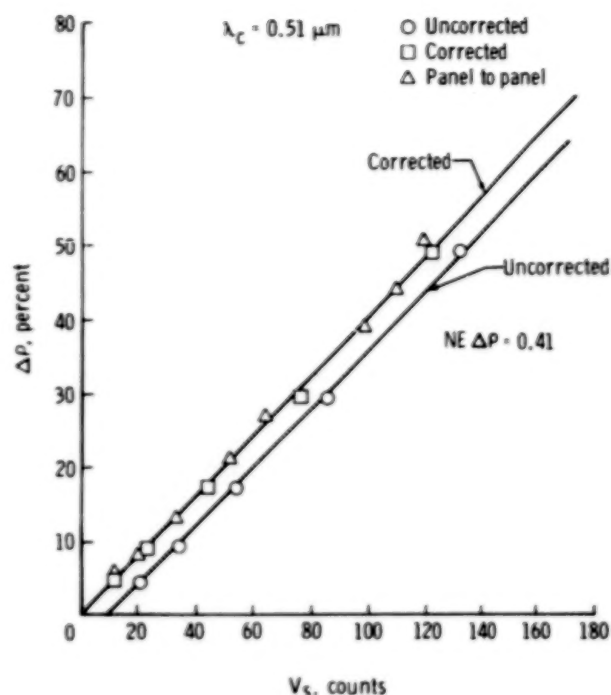


FIGURE 15.—Plot of relative reflectance as a function of scene signal voltage for channel 3 (September 25, 1975).

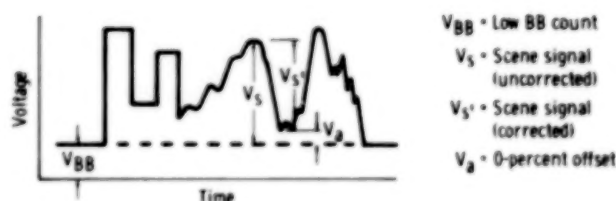


FIGURE 16.—Scanner video trace.

table for the extraterrestrial solar irradiance (table V).

An inspection of table IV reveals that for data Groups I and III, the P. Moon data more closely approximate the measured values than do the Ångström data. The Ångström values are closest for data Group IV, whereas the nomograph provides the best answers for data Groups I and II. Although the nomograph answers are not the best for Groups III and IV, there is more leeway for altering the numbers through the collection and use of more precise meteorological data. This adjustment would bring the measured and calculated numbers into better agreement.

One large source of error in calculating NE $\Delta\rho$ for the M²S is brought about by the separate optical paths of the ground scene and the calibration lamp.

The result is that the NER term used in the calculation is strongly influenced by the condition of the calibration optics, whereas the measured value of NE $\Delta\rho$ is not influenced at all by these optics. This result indicates a need to monitor the condition of these optics periodically and suggests that NER measurements would be better made using external sources.

Since making real-time measurements of NE $\Delta\rho$ in an operational sense is generally impractical, the question arises as to the relative merits of the various methods of calculating NE $\Delta\rho$. The answer depends on several considerations including the use that will be made of the data. Obviously, the P. Moon values are the correct order of magnitude and are easily accomplished, but the other calculations are capable of greater precision.

Generally, sensitivity data are used for "ball-park" estimates of performance and it appears the P. Moon values accomplish this satisfactorily. However, it would be constructive at this point to consider the magnitude of variations in NE $\Delta\rho$ that might occur because of such factors as time of year, time of day, latitude, and atmospheric conditions. This estimate can best be accomplished with the aid of the nomographs discussed previously.

Figure 7 indicates that at or near the summer solstice (June 21), the air mass m is nearly equal to 1.0 whatever the latitude, and this holds true for almost 2 hours before or after noon. Proceeding with this calculation for the data of June 2, 1978, channel 4 of the M²S, assuming clear conditions, one obtains for NE $\Delta\rho$ a value of about 0.16 percent, which compares with a measured value of 0.21 percent. The alteration of this number for hazy or exceptionally clear conditions is insignificant, but only near June. The situation can be vastly different, however, at the winter solstice (December 22). Again choosing channel 4, it can be seen that air mass m may vary from about 1.7 at 30° latitude (at noon) to about 2.75 at 45° latitude. This variance results in a variation in the nomograph number from 1.6 to 5.3. These numbers in turn translate to a change in NE $\Delta\rho$ of 0.31 to 1.0 percent. Additional changes will be brought about if the time is different from noon (as much as 42 percent in 2 hours), and this for a clear day. If haze is considered, the values for NE $\Delta\rho$ can range from 0.49 percent to nearly 2.0 percent at the two latitudes. For clarification, these values are given in table VIII.

TABLE VIII.—Possible Variations in Calculated Values of NE $\Delta\rho$ for Channel 4 of the M²S

NE $\Delta\rho$, percent	Local time	Month	Latitude, deg	Atmospheric condition
0.15	12 m. ^a	June	30	Haze to clear
.16	12 m.	June	45	Haze to clear
.31	12 m.	Dec.	30	Clear
.49	2 p.m.	Dec.	30	Clear
1.0	12 m.	Dec.	45	Clear
2.0	12 m.	Dec.	45	Haze
.95	2 p.m.	Dec.	30	Haze
1.2	12 m.	Oct.	45	Haze
.61	12 m.	Oct.	45	Clear

^a12 m. = noon.

It should be argued that in agricultural surveys, data are rarely taken beyond the month of October. Then, if a limitation is also placed on atmospheric conditions so that data are acquired under clear air conditions, a figure of 0.61 percent is found for noon at 45° latitude. The corresponding P. Moon value is 0.39, which is 36 percent less.

Conclusion

The purpose of calculating noise equivalent reflectance is generally to provide an approximate value to a potential data user for use in estimating sensor performance under field conditions. Considering the wide range of possible variations in noise equivalent reflectance that can be attributable to known conditions, as well as the influence of unknown, unpredictable, or time-varying conditions, it is believed that the P. Moon calculation provides the most convenient and usable indicator of performance. One outstanding reason for this conclusion is the simplicity in defining a standard procedure as opposed to defining standard conditions, with artificial compromises or constraining factors that would significantly complicate the procedure.

Situations may arise wherein the success of a particular experiment may be marginally dependent on the sensitivity of a scanner system under certain conditions. In such situations, a direct

measurement using reflectance panels is recommended. Otherwise, the nomograph described in this report should be used as the best indicator of system sensitivity.

Lyndon B. Johnson Space Center
National Aeronautics and Space Administration
Houston, Texas, July 16, 1979
953-36-00-00-72

Appendix A

Meteorological Effects on Radiation

An airborne scanner system collects radiant energy that has been reflected or emitted by a target on the surface of the Earth. The attenuation of solar radiation through the atmosphere from its extraterrestrial value is determined by the state of the atmosphere at any given time. The physical conditions of the airmass can be highly variable depending on temperature, humidity, dust content, etc. An exact model for radiation attenuation has not been developed, but approximations can be made in which the gross, average irradiance at the surface can be estimated. An extensive study on measured atmospheric quantities and radiation transfer models has been made (refs. 5, 7, 8, and 9). Only those features of interest to the current report will be discussed here, and the discussion is not to be considered as an exhaustive account.

In figure 17, consider a beam of parallel direct solar extraterrestrial spectral irradiance $H_{e\lambda}$ (watts per square centimeter per micrometer) at the top of a stratified atmosphere. For a parallel beam transmitted a distance dz , the irradiance will decrease by dH_{λ} , and assuming no radiant emittance within the distance dz , Schwarzschild's equation gives

$$\frac{dH_{\lambda}}{H_{\lambda}} = -k_{\lambda} dz \quad (A1)$$

where H_{λ} is the value of the irradiance at the top of the layer and k_{λ} is the volume extinction coefficient (attenuation coefficient including both absorption and scattering effects) (per kilometer). Integrating equation (A1) gives

$$H_{\lambda} = H_{\lambda_0} e^{-\int_0^z k_{\lambda} dz} \quad (A2)$$

and for a surface \overline{PN} at some angle to the zenith,

$$H_{\lambda} = H_{\lambda_0} \cos \theta_0 e^{-\int_0^x k_{\lambda} dx} \quad (A3)$$

However, $dx = \sec \theta dz$,

$$H_{\lambda} = H_{\lambda_0} \cos \theta_0 e^{-\sec \theta (\tau)} \quad (A4)$$

where

$$\tau = \int_0^{(\sec \theta)z} k_{\lambda} dz$$

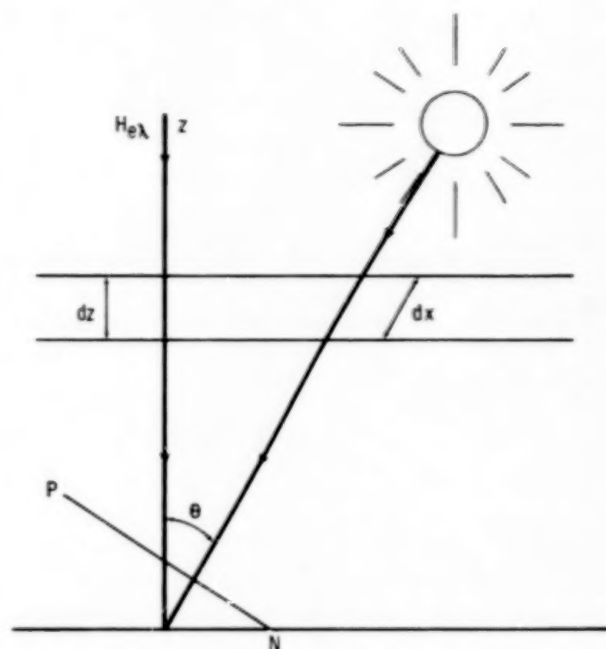


FIGURE 17.—Geometric relationships of solar irradiance quantities used in Schwarzschild's equation.

equals optical depth or thickness of the atmosphere. The quantity $\sec \theta$ is normally called the air mass m of the atmosphere. This can be seen by converting equation (A3) in terms of a mass extinction coefficient $\alpha_{\rho\lambda} = k_{\lambda}/\rho$, where ρ equals mass density. Letting dm equal mass element per unit area along a column of air in direction dx , one can write

$$\begin{aligned} dm &= \rho dx \\ &= \rho \sec \theta dz \end{aligned} \quad (A5)$$

Integrating and letting m_0 equal the mass per unit area in a vertical column,

$$m = (\sec \theta) m_0 \quad (A6)$$

Hence, $\sec \theta = m/m_0 = m_r$. Equation (A4) can now be written as

$$H_{\lambda} = H_{\lambda_0} \cos \theta_0 e^{-m_r \tau} \quad (A7)$$

In general, the optical depth is determined by both absorption and scattering. Ångström's atmospheric model for the visible spectrum (ref. 7) considers an average atmospheric state such that

$$\tau = \tau_R + \tau_a + \tau_w \quad (\text{A8})$$

where τ_R, τ_a is due to Rayleigh (molecular) scattering including corrections for refraction and anisotropy of the air molecules, haze, or dust scattering, and τ_w is the absorption due to water vapor, ozone, carbon dioxide, and other gases. Sometimes, the quantity $e^{-m\tau}$ is written as $e^{-m\tau} = (q_\lambda)^{m\tau}$, where $q_\lambda = e^{-\tau}$ and is termed the transmissivity of the atmosphere. For analysis of NE $\Delta\rho$, Ångström's model is used such that

$$H_\lambda = H_{\lambda_0} \cos \theta_0 e^{-m\tau_R} e^{-m\tau_a} e^{-\tau_w} \quad (\text{A9})$$

where $\tau_R = a_R$ (Rayleigh extinction coefficient)
 $a_R = 0.00889\lambda^{-4.05}$ for λ in micrometers
 $\tau_a = a_a$ (dust, haze extinction coefficient)
 $a_a = 2.303B(2\lambda)^{-\alpha}$ for λ in micrometers
 $\tau_w = a_w$ (absorption extinction coefficient)

To fit the modular multispectral scanner data for latitude 45° N (the position of the panels), the average turbidity B for this latitude and absorption a_w are found in charts given in references 5 and 8. Finally, for a_a , the normal value of α for haze scattering is taken as 1.5. As the haze particles change in size and number per unit volume, α will lie between $0 \leq \alpha \leq 4$, where for 1-micrometer size particles, $\alpha \approx 0.5$.

One other atmospheric effect must be included to obtain the total spectral irradiance on a target on

the Earth's surface, and that is the irradiance due to multiple scattering of light within the atmosphere. As might be expected, this diffuse sky irradiance S_λ is highly variable and no satisfactory atmospheric model fits experimental data taken at various locations. Models of S_λ have been determined using scattering functions in the radiation transfer equation (ref. 5), and the concept is expressed by the simple formula

$$\frac{S_\lambda}{H_\lambda} = k \cos \theta_0 \quad (\text{A10})$$

where $k = k(\tau_R, \tau_a, m)$ and H_λ is the direct solar irradiance at the surface. Hence, the total irradiance $H_{s\lambda}$ of a target scene is given by

$$H_{s\lambda} = H_{\lambda_0} \cos \theta_0 e^{-m\tau(\tau_R + \tau_a)} e^{-\tau_w} + S_\lambda \quad (\text{A11})$$

Another useful atmospheric model used in finding optical depths in terms of the horizontal visual range is found in reference 10. In this model, the aerosol (haze) optical depth τ_a is related through the turbidity of the atmosphere and the volume extinction coefficient to the horizontal visual range. The calculated Rayleigh scattering and aerosol optical depths as a function of wavelength and visual range are shown in figures 5 and 6. These were used in calculating the range of values for the ratio of system parameters $[H_e/\pi][NE \Delta\rho/NER]$ shown in figures 8, 9, and 10. In addition, the ratio of sky irradiance to direct solar irradiance was taken as

$$\frac{S_\lambda}{H_\lambda} = k(\tau_R, \tau_a, m) \cos \theta_0 \quad (\text{A12})$$

$$\frac{S_\lambda}{H_\lambda} = e^{\tau_R + \tau_a} - \frac{0.68}{m} \quad (\text{A13})$$

Appendix B—Symbols

A_c	collecting area, cm^2	$H_{s\lambda}$	total irradiance of target scene
A_t	target area, cm^2	H_t	total target irradiance, $\text{W}\cdot\text{cm}^{-2}$
a_a	aerosol attenuation coefficient	$H_{\Delta\lambda}$	solar irradiance, $\text{W}\cdot\text{m}^{-2}\cdot\mu\text{m}^{-1}$ (table I)
a_R	Rayleigh extinction coefficient	H_λ	spectral irradiance, $\text{W}\cdot\text{cm}^{-2}\cdot\mu\text{m}^{-1}$
a_w	water-vapor absorption coefficient	$H_{\lambda\perp}$	spectral normal irradiance
B	turbidity coefficient, $0.05 \leq B \leq 0.2$	H_0	extraterrestrial solar irradiance; solar constant, $\text{W}\cdot\text{m}^{-2}$ (table I)
$D(0-\lambda)$	percentage of solar constant associated with wavelengths shorter than λ (table V)	h	hemisphere
dA	element of area, cm^2	$k = qm - 0.68$	
dH_λ	decrease in irradiance	k_λ	volume extinction coefficient, km^{-1}
dm	mass element per unit area in direction dx	m	absolute air mass, unitless; approximately equal to secant θ for low altitudes and for $0^\circ \leq \theta \leq 60^\circ$
dP_i	power incident on surface	$m_r = m/m_0$	relative air mass, unitless
dP_r	power reflected from surface	$= \sec \theta$	
$dx = \sec \theta dz$		m_0	mass per unit area in vertical column
dz	beam transmission distance	N	radiance (power radiated), $\text{W}\cdot\text{cm}^{-2}\cdot\text{sr}^{-1}$
$d\Omega$	projected solid angle	N_a	backscatter radiance, $\text{W}\cdot\text{cm}^{-2}\cdot\text{sr}^{-1}$
$E(\lambda)$	solar spectral irradiance averaged over small bandwidth centered at λ , $\text{W}\cdot\text{m}^{-2}\cdot\mu\text{m}^{-1}$ (table V)	N_{cal}	radiance produced by calibration lamp
$E(0-\lambda)$	area under solar spectral irradiance curve in wavelength range 0 to λ , $\text{W}\cdot\text{m}^{-2}$ (table V)	N_p	target radiance, computed from table I (P. Moon), $\text{W}\cdot\text{cm}^{-2}\cdot\text{sr}^{-1}$
H	irradiance (power density), $\text{W}\cdot\text{cm}^{-2}$	N_r	path radiance due to scattering into beam from surrounding targets
H_a	irradiance, Ångström's model, $\text{W}\cdot\text{cm}^{-2}$	$N_{r\lambda}$	path spectral radiance due to scattering of radiation into the beam from surrounding ground targets
H_b	total irradiance from all sources, $\text{W}\cdot\text{cm}^{-2}$	N_s	scene radiance, $\text{W}\cdot\text{cm}^{-2}\cdot\text{sr}^{-1}$
H_e	extraterrestrial solar irradiance, Turner's model	N_t	target radiance, $\text{W}\cdot\text{cm}^{-2}\cdot\text{sr}^{-1}$
H_{eb}	extraterrestrial solar irradiance in given spectral band, $\text{W}\cdot\text{cm}^{-2}$	$N_{t\lambda}$	scene or target spectral radiance
H_{ex}	extraterrestrial spectral solar irradiance, $\text{W}\cdot\text{cm}^{-2}\cdot\mu\text{m}^{-1}$	N_λ	spectral radiance, $\text{W}\cdot\text{cm}^{-2}\cdot\text{sr}^{-1}\cdot\mu\text{m}^{-1}$
$H_{e\lambda}$	parallel direct solar extraterrestrial spectral irradiance, $\text{W}\cdot\text{cm}^{-2}\cdot\mu\text{m}^{-1}$	$N_\lambda(\text{cal})$	calibration source spectral radiance
H_g	ground irradiance, $\text{W}\cdot\text{cm}^{-2}$	NER	noise equivalent radiance, $\text{W}\cdot\text{cm}^{-2}\cdot\text{sr}^{-1}$
$H_{g\lambda}$	ground spectral irradiance	NER_λ	spectral noise equivalent radiance
H_p	target irradiance from table I (P. Moon), $\text{W}\cdot\text{cm}^{-2}$		

NE $\Delta\rho$	noise equivalent reflectance, unitless	ρ	total reflectance; mass density (eq. (A5))
P_i	power incident, W	ρ'	partial reflectance, sr^{-1}
P_{in}	power input, W	ρ_{cal}	calibration reflectance
P_r	power reflected, W	ρ_{eq}	equivalent scene reflectance
\overline{PN}	surface at some angle to the zenith (fig. 17)	ρ_n	noise reflectance
$q = e^{\tau_R + \tau_a}$		ρ_s	signal reflectance
$q_\lambda = e^{-\tau}$	transmissivity of atmosphere	ρ_0	a selected value of reflectance
$R = V_s/N_s$	scanner system responsivity, $\text{V} \cdot (\text{W} \cdot \text{cm}^{-2} \cdot \text{sr}^{-1})^{-1}$ (eq. (41))	τ	optical depth (optical thickness) of atmosphere
R_v	visual range	$\tau_a = a_a$	aerosol (haze) optical depth
S	sky irradiance, $\text{W} \cdot \text{cm}^{-2}$	$\tau_R = a_R$	total Rayleigh optical depth
S_b	diffuse sky irradiance in given spectral band pass	$\tau_w = a_w$	absorption due to water vapor and other gases (eq. (A8))
S_t	sky irradiance for Turner's equation, $\text{W} \cdot \text{cm}^{-2}$	ϕ_r	azimuth angle of reflected solar energy, deg
S_λ	diffuse or sky spectral irradiance for Ångström's equation, $\text{W} \cdot \text{cm}^{-2} \cdot \mu\text{m}^{-1}$	Ω	solid angle of reflectance, sr
$S/N = V_s/V_n$	signal-to-noise ratio, unitless	ω	solid viewing angle, instantaneous field of view, sr
T	time, hours	Subscripts:	
V	emf, V	a	aerosol
V_a	zero-percent offset emf, V	BB	blackbody
V_{BB}	emf, low blackbody count, V	b	band (band pass)
V_{cal}	calibration emf, V	c	collecting (collector); center
V_n	noise emf, V	cal	calibration
V_s	scene signal emf, uncorrected, V	e	extraterrestrial
V'_s	scene signal emf, corrected, V	eb	extraterrestrial in given band
V_1, V_2	scanner output emf from targets 1 and 2, V	eq	equivalent
x, y, z	rectangular Cartesian coordinates	ex	extraterrestrial
$\alpha_{\rho\lambda} = k_\lambda/\rho$	mass extinction coefficient	g	ground
Δ	change	h	hemisphere
ΔN_s	change in scene radiance	i	incident
ΔN_λ	change in spectral radiance	in	input
$\Delta\rho$	change in scene reflectance	n	noise
θ	nadir angle, deg	p	P. Moon
θ_r	nadir angle of reflected solar energy, deg	R	Rayleigh
θ_0	nadir angle of incident solar energy, deg	r	reflected; relative
λ	wavelength, μm	s	scene (signal)
λ_c	center wavelength, μm	t	target; Turner
λ_0	a selected wavelength, μm	v	visual
		w	water vapor; water vapor and other gases
		λ	wavelength

ρ	mass density
0	reference (selected)

Superscripts:

m	relative air mass
α	Ångström's exponent, $0 < \alpha \leq 4$

References

1. Hudson, R. D.: Infrared System Engineering. Wiley-Interscience, 1969.
2. Wolfe, William L., ed.: Handbook of Military Infrared Technology. Office of Naval Research, Department of the Navy, U.S. Government Printing Office, 1965.
3. Hulstrom, R. L.: Spectral Measurements and Analyses of Atmospheric Effects on Remote Sensor Data. Scanners and Imagery Systems for Earth Observation; Proceedings of the Seminar, San Diego, Calif., Aug. 19, 20, 1974. Society of Photo-Optical Instrumentation Engineers (Palos Verdes Estates, Calif.), 1975, pp. 90-100.
4. Valley, Shea L., ed.: Handbook of Geophysics and Space Environments. Air Force Cambridge Research Laboratories, 1965.
5. Robinson, Nathan, ed.: Solar Radiation. Elsevier Pub. Co., 1966.
6. Thekaekara, M. P.: Evaluating the Light From the Sun. Optical Spectra, vol. 6, Mar. 1972, pp. 32-35.
7. Turner, Robert E.: Atmospheric Effects in Multispectral Remote Sensor Data. Final Technical Report, 15 May 1974—14 Mar. 1975. NASA CR-141863, 1975.
8. Kondrat'ev, K. Ia., ed.: Radiation Characteristics of the Atmosphere and the Earth's Surface. NASA TT F-678, 1973.
9. Turner, Robert E.: Radiative Transfer in Real Atmospheres. Technical Report, 1 Feb.—31 Oct. 1973. NASA CR-140199, 1974.
10. Horvath, R.; Spencer, M.; and Turner, R.: Atmospheric Correction and Simulation of Space Acquired Remote Sensor Data: 0.4 to 1.0-Micron Spectral Range. Willow Run Laboratory Rep. WRL 10657-5-F (Contract NAS9-12269), July 1972.

1. Report No. NASA TP- 1575		2. Government Accession No.		3. Recipient's Catalog No.	
4. Title and Subtitle DETERMINATION OF NOISE EQUIVALENT REFLECTANCE FOR A MULTISPECTRAL SCANNER—A SCANNER SENSITIVITY STUDY				5. Report Date December 1979	
				6. Performing Organization Code	
7. Author(s) Daniel E. Gibbons, Fort Lewis College, and Richard R. Richard, JSC				8. Performing Organization Report No. S-497	
9. Performing Organization Name and Address Lyndon B. Johnson Space Center Houston, Texas 77058				10. Work Unit No. 953-36-00-00-72	
				11. Contract or Grant No.	
12. Sponsoring Agency Name and Address National Aeronautics and Space Administration Washington, D.C. 20546				13. Type of Report and Period Covered Technical Paper	
				14. Sponsoring Agency Code	
15. Supplementary Notes					
16. Abstract <p>The methods used to calculate the sensitivity parameter noise equivalent reflectance of a remote-sensing scanner are explored, and the results are compared with values measured over calibrated test sites. Data were acquired on four occasions covering a span of 4 years and providing various atmospheric conditions. One of the calculated values is based on assumed atmospheric conditions, whereas two others are based on atmospheric models. It was found that the assumed atmospheric conditions provide useful answers adequate for many purposes. A nomograph is developed to indicate sensitivity variations due to geographic location, time of day, and season.</p>					
17. Key Words (Suggested by Author(s)) Remote sensors Nomographs Electromechanical scanners Scanning radiometers Sensor resolution				18. Distribution Statement STAR Subject Category: 35 (Instrumentation and Photography)	
19. Security Classif. (of this report) Unclassified		20. Security Classif. (of this page) Unclassified		21. No. of Pages 31	
				22. Price* \$4.00	

*For sale by the National Technical Information Service, Springfield, Virginia 22161

